The Canadian Mineralogist
Vol. 39, pp. 957-978 (2001)

GEOCHEMISTRY AND MINERALOGY OF GOLD-RICH HYDROTHERMAL PRECIPITATES FROM THE EASTERN MANUS BASIN, PAPUA NEW GUINEA

ROGER MOSS[§] AND STEVEN D. SCOTT

Scotiabank Marine Geology Research Laboratory, Department of Geology, University of Toronto, 22 Russell Street, Toronto, Ontario, Canada M5S 3B1

ABSTRACT

Three of the five hydrothermal vent fields currently known in the Manus back-arc basin of Papua New Guinea are enriched in gold. Samples of precipitates from the PACMANUS and Susu Knolls hydrothermal fields in eastern Manus Basin contain up to 56.8 ppm gold, and average 11.3 ± 13 (1σ) ppm (n = 103). Chimney samples dominated by sphalerite, barite and chalcopyrite have significantly higher contents of gold than sulfide-poor samples. Gold in the sulfide chimneys occurs as micrometric grains of silver-poor (1.4 to 4.2 wt.% Ag) native gold in three distinct associations. In copper-rich chimney samples, gold occurs as inclusions in chalcopyrite associated with tennantite, bornite and covellite. In zinc-rich chimney samples, gold is present mainly as inclusions in tennantite associated with chalcopyrite and sphalerite. A high activity of sulfur is indicated for the gold-rich eastern Manus Basin precipitates by the sulfide assemblages, the low iron content of sphalerite (average = 2.3 ± 3 mole % FeS), and the silver-poor nature of gold grains. Evaluation of possible complexes of gold indicates that AuHS° is the dominant complex, which is consistent with the high activity of sulfur in the hydrothermal system. According to available experimental data, AuHS° is the dominant complex up to 325°C. This complex thus is the only one required for gold enrichment in both the Zn–Au and the Cu–Au associations. Gold transport as the AuHS° complex is likely to be equally important in other seafloor hydrothermal systems with acidic end-member hydrothermal fluids.

Keywords: hydrothermal, gold, vent, seafloor, massive sulfide, PACMANUS vent field, Papua New Guinea.

SOMMAIRE

Trois des cinq champs d'évents hydrothermaux connus dans l'arrière-arc du bassin de Manus, en Papouasie Nouvelle Guinée, montrent un enrichissement en or. Les échantillons des précipités provenant des champs hydrothermaux de PACMANUS et de Susu Knolls, dans le secteur oriental du bassin de Manus, contiennent jusqu'à 56.8 ppm d'or, et atteignent en moyenne 11.3 ± 13 (1σ) ppm (n = 103). Les échantillons de cheminées à prédominance de sphalérite, barite et chalcopyrite contiennent des teneurs en or nettement plus élevées que les échantillons à faible teneur en sulfures. L'or des cheminées sulfurées se présente sous forme de grains micrométriques d'or natif à faible teneur en argent (de 1.4 à 4.2% Ag, poids), en trois associations distinctes. Dans les échantillons de cheminées riches en cuivre, l'or se présente sous forme d'inclusions dans la chalcopyrite associée à la tennantite, la bornite et la covellite. Dans les échantillons de cheminées riches en zinc, l'or se présente surtout sous forme d'inclusions dans la tennantite associée à la chalcopyrite et la sphalérite. Dans le secteur oriental du bassin de Manus, une activité élevée en soufre serait indiquée pour expliquer ces précipités aurifères associés à des assemblages riches en sulfures, la faible teneur en fer de la sphalérite (en moyenne 2.3 ± 3% FeS, base molaire), et la faible teneur en argent des grains d'or. Une évaluation des complexes potentiels pour transporter l'or montre que AuHS° est le plus important, ce qui concorde avec l'activité accrue du soufre dans le système hydrothermal. Selon les données expérimentales disponibles sur la stabilité de ces complexes, AuHS° serait prédominant jusqu'à 325°C. Il serait donc le seul requis pour expliquer l'enrichissement en or à la fois dans les associations Zn–Au et Cu–Au. Le transfert de l'or sous forme du complexe AuHS° serait également important dans d'autres milieux d'évents hydrothermaux dont les fluides s'approchent du pôle acide.

(Traduit par la Rédaction)

Mots-clés: hydrothermal, or, évent, fonds marins, sulfures massifs, champ d'évents PACMANUS, Papouasie Nouvelle Guinée.

§ *E-mail address*: roger_moss@sympatico.ca

Introduction

Exploration of the modern seafloor over the past two decades has resulted in the discovery of many areas of hydrothermal activity in geographically and tectonically diverse settings. Initial work between 1977 and 1985 concentrated on the investigation of vent sites on the mid-ocean ridges of the East Pacific, and on the Mid-Atlantic Ridge. Hydrothermal precipitates from several of these ocean-ridge deposits were found to be enriched in gold (Hannington & Scott 1988, 1989a, Hannington *et al.* 1986, 1991), although such gold-rich precipitates are not typical of the majority of ocean-ridge deposits.

More recently, attention has turned to the submarine arcs and marginal basins of the western Pacific. This exploration has resulted in the identification of more than 27 hydrothermal sites (Ishibashi & Urabe 1995) ranging in water depth from the shallow-water (~ 200 m) Whakatane vent site south of White Island, New Zealand (Hannington *et al.* 1999) to the 3,700-meter-deep Alice Spring site in the central Mariana Trough (Craig *et al.* 1987a). Many of the precipitates associated with these vent sites are extremely gold-rich, with values up to 71 ppm Au (average 28 ppm, $n = 11$) reported for sulfides from the Suiyo Seamount on the Izu–Bonin arc (Watanabe & Kajimura 1994), and up to 49 ppm Au (average 20 ppm, $n = 37$) from the Sunrise Deposit, 400 km to the south (Iizasa *et al.* 1999). Clearly, the prolific gold mineralization found on land in the volcanic arcs of the region (Sillitoe 1989) continues into the submarine arcs, forearcs and back-arc basins associated with these subaerial environments.

Our understanding of the processes involved in the enrichment of gold in volcanogenic massive sulfide deposits has been shaped by complementary studies on both the modern seafloor (*e.g.*, Hannington & Scott 1989a, b, Hannington *et al.* 1991, 1995, Herzig *et al.* 1993) and ancient deposits on land (*e.g.*, Huston & Large 1989, Hutchinson 1990, Large 1990, Huston *et al.* 1992). In this study of gold-rich precipitates from the eastern Manus Basin, Papua New Guinea, we describe the geochemistry and mineralogy of gold in hydrothermal precipitates from the PACMANUS and Susu Knolls vent fields, two of the most gold-rich back-arc basin deposits of the western Pacific.

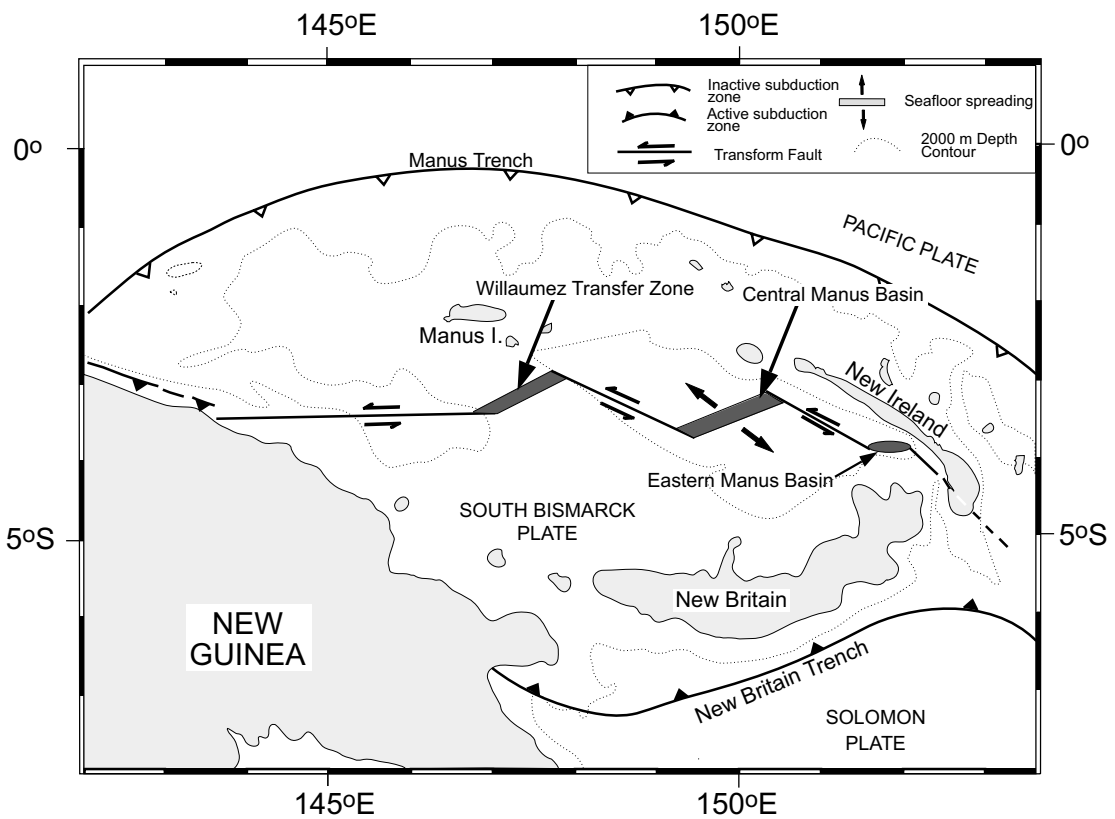

FIG. 1. Main tectonic elements of the Manus Basin region (modified from Benes *et al.* 1994).

Geological Setting

The Manus Basin is the back-arc of the active New Britain volcanic arc, situated to the east of the island of New Guinea (Fig. 1). Subduction began under New Britain after earlier subduction along the Manus trench stopped in the Oligocene owing to the effect of the Ontong Java Plateau docking against the Manus trench (Martinez & Taylor 1996). Back-arc spreading occurs along the central Manus spreading center, decreasing from 92 mm/year (full rate) in the southwestern end of the spreading center to 0 mm/year in the northeast (Martinez & Taylor 1996). Eastern Manus Basin is a pull-apart structure that consists of a series of *en échelon* volcanic ridges between two transform faults within thinned arc crust (Binns & Scott 1993). Development of this structure is believed to have been contemporaneous with that of the Bismarck microplate (Martinez & Taylor 1996).

Four active vent fields and one inactive field have been discovered in Manus Basin, three of which occupy an area of approximately 4,000 km^2 in the eastern Manus Basin (Binns *et al.* 1997). The inactive deposit is located on the Willaumez transfer zone, and consists primarily of iron oxide mounds (Binns 1994). The Vienna Woods hydrothermal field occurs at a depth of 2,500 meters on the central Manus spreading center. The first reports of hydrothermal activity in the region resulted from deep camera tows, which photographed vent fauna and inactive chimneys (Both *et al.* 1986). Active hydrothermal venting was discovered on the central Manus spreading center during the OLGA II research cruise of the RV Sonne (Tufar 1990). Both black and white smoker chimneys with abundant vent fauna were found. The vent field consists predominantly of zinc-rich chimneys, venting 285° to 300°C fluid, sitting atop a sulfide mound, with fewer anhydrite-rich chimneys sitting directly on the seafloor (Auzende *et al.* 1996a, b). Hydrothermal precipitates are enriched in zinc sulfide (sphalerite and wurtzite) and silica with an average base-metal content of 29.7% Zn, 2.2% Cu and 0.6% Pb (n = 25, Tufar 1990). These sulfides also are enriched in gold (average 30 ppm) and silver, which ranges from 25 ppm to 1036 ppm (Binns 1994).

The discovery of CH_4 and ^{3}He anomalies in the water column (Craig & Poreda 1987, Craig *et al.* 1987b) was the first indication of hydrothermal activity in the eastern part of Manus Basin. Subsequently, three main vent fields, DESMOS, Susu Knolls and PACMANUS, were found in the region. DESMOS is a cauldron within basaltic andesite over which a large methane and manganese plume was discovered in 1990 (Sakai 1991, Gamo *et al.* 1993). Low-temperature (118°C), acidic (pH = 2.1), vigorous venting is associated with a fault in the northwest wall of the cauldron (Auzende *et al.* 1996a, b). This vent site, named Onsen (Fig. 2), is characterized by a high sulfate content in the vent fluid and the deposition of abundant native sulfur (Gamo *et al.* 1997). Mineralization consists of enargite and pyrite associated with alunite (Gena *et al.* 1998), suggesting similarities with the subaerial to shallow submarine high-sulfidation deposits described by Hannington *et al.* (1999).

The Susu Knolls vent field, discovered during the 1996 PACMANUS III expedition in the eastern part of the eastern Manus Basin, is situated on a northwest–southeast-trending andesitic ridge named Tumai Ridge. The vent field consists of clusters of vigorously active chimneys on the tops of two coalesced porphyritic dacite domes (North Su and South Su), and an adjacent site of chimneys and massive sulfides known as Suzette (Fig. 2). The mineralization at Suzette is particularly

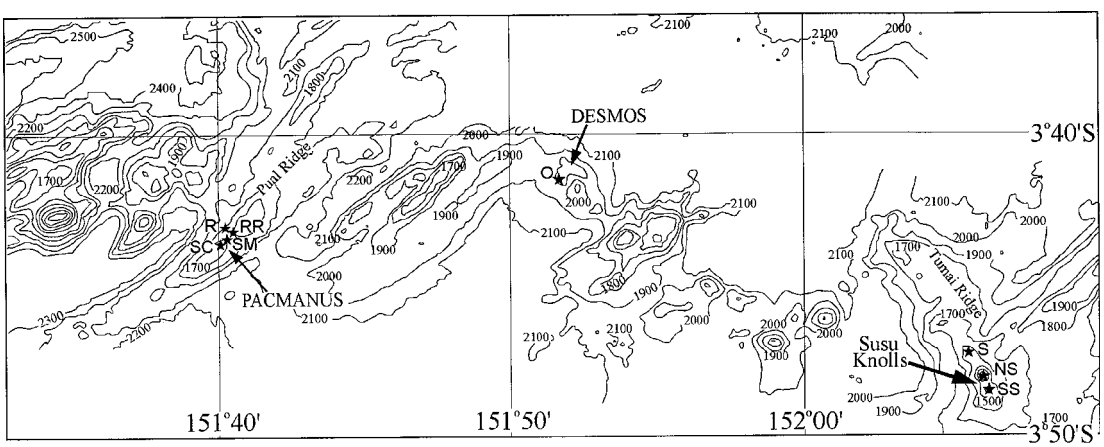

FIG. 2. Simplified bathymetric map of eastern Manus Basin (after Sakai 1991) showing location of vent sites (stars). Abbreviations: R Rogers Ruins, RR Roman Ruins, SC Snowcap, SM Satanic Mills, O Onsen, S Suzette, NS North Su, SS South Su.

copper-rich, with an average of 19% Cu reported from three chimneys. The three samples reported to date also have high contents of zinc (average 22%), silver (average 125 ppm) and gold (average 23 ppm) (Binns *et al.* 1997).

The PACMANUS vent field was discovered in 1991 (Binns & Wheller 1991), underlying a strong Mn anomaly in the water column (Sakai 1991). It is situated near the bathymetric minimum of a northeast–southwest-trending ridge named Pual Ridge, which is composed of andesite, dacite and rhyolite. Andesite dominates the lower reaches of the 500-meter-high ridge, whereas the crest is predominantly dacite and rhyolite (Binns & Scott 1993, Scott & Binns 1995). Detailed investigations of the area by deep-tow camera and video (Binns & Wheller 1991, Binns & Scott 1993) and submersible (Auzende *et al.* 1996a, b) revealed four discrete vent-sites (Fig. 2), separated by areas of intermittent hydrothermal activity in the form of iron–manganese oxides and low-temperature shimmering vents. This hydrothermal activity covers an area of approximately 1100 × 600 meters on the crest of Pual Ridge.

The Rogers Ruins vent site, located at the northern edge of the ridge crest, consists of actively venting black smokers up to 7.5 meters high, together with inactive chimneys. Active chimneys have complex shapes, many with peripheral spires growing around a dominant central structure. Samples from the vent field are dominantly zinc-rich with iron oxide coatings. Immediately to the east of the vent field, numerous small (approximately one meter diameter) mounds of iron and manganese oxides are venting clear, low-temperature (40°C) fluid.

The Roman Ruins vent site lies approximately 250 meters to the south of Rogers Ruins, and consists of numerous large (up to 20 meters high and 3 meters in diameter) predominantly inactive chimneys. Many such chimneys appear to have coalesced to form a chimney "wall", with active venting of clear hydrothermal fluid from small chimneys and fissures on ledges in this "wall".

Coalesced chimney structures venting high temperature (up to 268°C) fluid through small "chimneylets" are characteristic of the Satanic Mills site. In contrast to samples collected from Roman Ruins and Rogers Ruins, those from Satanic Mills tend to be copper-rich.

The fourth vent site, Snowcap, covers a knoll of altered dacite–rhyolite and is characterized by low-temperature diffuse venting and abundant white bacterial mat associated with altered hyaloclastite (Binns *et al.* 1997). Active chimneys with beehive-type diffuser tops (*cf.* Fouquet *et al.* 1993) are located immediately south of this site.

Analytical Techniques

A total of 103 chimney samples and sub-samples were analyzed during this study. Samples were recovered by dredging during three RV Franklin cruises (PACMANUS II, III and IV) and by Shinkai 6500 submersible during the 1995 Manusflux cruise. Concentrations of copper, lead, silica and calcium were obtained by X-ray fluorescence (XRF), of sulfur by the LECO infrared spectrometry technique, and of bismuth, tellurium and selenium by hydride generation followed by inductively coupled plasma – atomic emission spectrometry (ICP–AES), all at Activation Laboratories, Ancaster, Ontario. Concentrations of the remaining elements reported here, including gold, were established by instrumental neutron activation analysis (INAA) at the University of Toronto. Details of the analytical procedure are given in Moss & Scott (1996).

Analyses of gold and sphalerite were carried out using a Cameca SX–50 electron microprobe. A synthetic gold–silver alloy ("electrum") standard with 20 at.% Ag was used to analyze for gold and a synthetic sphalerite standard containing 20 at.% Fe was used for the sphalerite analyses. Repeat analyses of these standards indicate relative precisions [(standard deviation/mean) × 100] of 2% for Au, 3% for Ag, 0.3% for Zn, 0.7% for Fe and 0.1% for S. X-ray powder diffraction was performed at the Department of Chemistry, University of Toronto, with a Siemens D5000 diffractometer operating at 50 kV, 35 mA.

Bulk Composition of Hydrothermal Precipitates

The samples analyzed during this study include hydrothermal precipitates from the four PACMANUS vent sites and the three sites in the Susu Knolls area (Table 1). The gold content of the precipitates ranges from below detection (approximately 4 ppb) to 56.8 ppm and averages 11.3 ppm (Table 2). Precipitates from Roman Ruins (average 17.2 ± 13 ppm Au, n = 37), Susu Knolls (average 14.8 ± 18 ppm Au, n = 9) and Satanic Mills (average 13.3 ± 11 ppm Au, n = 25) are clearly more gold-rich than those from Snowcap (average 2.3 ± 3 ppm Au, n = 13) and Rogers Ruins (average 1.3 ± 4 ppm Au, n = 18) (Fig. 3a). This difference in gold content is reflected in the mineralogical composition of the precipitates, which is controlled by the physical and chemical characteristics of the hydrothermal fluid. Temperatures of the vent fluid measured during the ManusFlux Cruise averaged 245°C at the Satanic Mills vent site, and 160°C at Roman Ruins (Auzende *et al.* 1996b, Gamo *et al.* 1997). Higher temperatures, up to 285°C, were measured for the Susu Knolls vent sites during the 2000 Manaute Cruise (Y. Fouquet, pers. commun., 2000), consistent with the more copper-rich nature of samples from the Suzette vent site than those from the PACMANUS area.

Samples to be analyzed were selected to represent the range of mineralogical types occurring in the region, and were distinguished according to their dominant mineral assemblage. Oxidized chimneys rich in iron oxide and silica from the Rogers Ruins vent site at

TABLE 1. DESCRIPTION OF SULFIDE SAMPLES FROM VARIOUS VENT-SITES IN THE EASTERN MANUUS BASIN

Satanic Mills

297-S-2A	Piece of black smoker chimney, actively venting 220°C fluid when sampled, with numerous chalcopyrite-lined orifices and a thin Fe-oxide exterior crust.
297-S-2B	Two pieces of chimney from same area as 2A. Chalcopyrite-lined conduits are common. Some conduits are lined by sphalerite.
297-S-5	Pieces of sphalerite-rich chimney, with chalcopyrite-lined conduits.
301-S-01	Inactive chimney near a 250°C black smoker. Massive chalcopyrite, sphalerite and pyrite clog two orifices, and one has an iron oxide coating. The chimney exterior has a thin layer of Fe-oxide covered by manganese oxide.
301-S-02	Inactive chimney sampled near a 268°C black smoker. Interior consists of three coalesced orifices lined with euhedral coarse-grained sphalerite.
118310	Crusts rich in iron oxide and manganese oxide on hyaloclastite.
118355C	Zoned chalcopyrite–barite–sphalerite piece.
118553	Piece of chimney rich in sphalerite and Fe-oxide.
118554A	Bottom of sphalerite-rich chimney.
118554B	Sphalerite-rich piece of chimney.
118555-2 to 7	Cross-sections through a sphalerite-rich chimney.
118556C-1	Chalcopyrite-rich inner zone of zoned chimney.
118556C-2	Outer zone of chimney, rich in sphalerite and barite.
118565	Piece of chimney rich in Fe-oxide and barite.
118567	Zoned chalcopyrite – Fe-oxide piece of chimney.
118584A-1	Chalcopyrite-rich orifice.
118584A-2	Sphalerite-rich piece of chimney.
118584A-3	Zoned piece from chalcopyrite-rich interior to Fe-oxide exterior.
118584B1A	Massive chalcopyrite (to 1 cm) occurs around a small (1 cm diameter) orifice in the chalcopyrite-rich portion of chimney, with some sphalerite near exterior.
118587D	Piece of chimney rich in sphalerite and barite.
132450	Section through a chalcopyrite-rich chimney with clogged orifices 1 to 5 mm in diameter.
132451	Section through chimney rich in pyrite and sphalerite.
132452	Piece of sphalerite-rich chimney.
132453	Piece of chalcopyrite-rich chimney.
132453-1	Basal section of chalcopyrite-rich chimney.

Rogers Ruins

132552	Portion of sphalerite–barite rich chimney with minor iron oxide.
132557	Sphalerite–barite-rich piece of chimney.
132557-1	Inner chimney wall.
132557-2	Inner middle chimney wall.
132557-3	Outer middle chimney wall.
132557-4	Exterior chimney wall.
132579	Silica – iron oxide-rich piece of chimey.
132649	Silica – iron oxide-rich piece of chimney.
132651	Piece of iron oxide mound with a thin manganese-oxide-rich exterior.
132651-1	Manganese-oxide-rich exterior part of mound.
132651-2	Iron-oxide-rich interior part of iron–manganese oxide mound.
132652	Sphalerite–barite-rich piece of chimney flange.
132720	Iron-oxide-rich precipitate with manganese oxide coating.
132740	Iron-oxide-rich sample with minor manganese oxide crust.
132744	Fragment of oxidized chimney dominated by iron oxide.
133990	Iron-oxide-rich crust.
134293	Cross section through a sphalerite–barite-rich piece of chimney.
134296	Portion of beehive-type diffuser, with alternating sphalerite and silica-rich layers.

Suzette

132807-1	Chalcopyrite–barite-rich inner portion of zoned chimney.
132807-2	Sphalerite–barite-rich outer portion of chimney with a thin iron oxide coating.
133012	Chalcopyrite-rich chimney with a thin (1 to 2 mm thick) sphalerite rim covered by iron oxide and a large central orifice filled with sphalerite and barite.
133016	Section through a sphalerite-rich composite chimney with three orifices.
133021	Zoned chimney with an interior chalcopyrite-rich zone (1–5 mm), a middle sphalerite-rich zone (5–15 mm) and an outer iron-oxide – atacamite zone (0.5–1 mm).

North Su

133870	Chalcopyrite–barite-rich piece of chimney.
133880	Chalcopyrite–pyrite-rich piece of chimney.

Roman Ruins

301-S-03	Small pieces of sphalerite-rich chimney with a massive sphalerite interior and a thin layer of Fe-oxide on the exterior.
304-S-01	Chimney pieces from a small active diffuser venting clear 179°C fluid. Samples have a sphalerite-rich interior, with some pyrite, and an iron oxide exterior coating.
132376	Chimney fragment with a massive chalcopyrite interior and a thin (<1 cm) sphalerite-rich exterior covered by a 1-mm-thick Fe-oxide layer.
132616-1	Chalcopyrite-rich central portion of a zoned chimney.
132616-2	Sphalerite-rich portion of zoned chimney.
132616-3	Mixed chalcopyrite– sphalerite central orifice of chimney.
132620	Zoned chalcopyrite – sphalerite – iron oxide chimney.
132620-1	Middle sphalerite-rich piece.
132620-2	Exterior iron-oxide-rich piece.
132620-4	Middle sphalerite-rich piece.
132620-5	Interior massive chalcopyrite piece.
132620-6	Interior massive chalcopyrite piece.
132620-7	Interior massive chalcopyrite piece.
132620-8	Interior mixed chalcopyrite-sphalerite.
132620-9	Interior massive chalcopyrite.
132620-10	Middle sphalerite-rich piece.
132620-11	Chalcopyrite-rich orifice rim.
132620-12	Middle sphalerite-rich piece.
132620-13	Exterior iron-oxide rich piece.
132620-14	Middle sphalerite-rich piece.
132620-15	Middle sphalerite-rich piece.
132620-16	Middle sphalerite-rich piece.
132620-17	Massive chalcopyrite rim of secondary orifice.
132620-18	Exterior chalcopyrite–sphalerite-rich piece.
132620-19	Exterior chalcopyrite-rich piece.
132620-20	Exterior sphalerite-rich piece.
132620-21	Exterior sphalerite-rich piece.
132621	Section through a chalcopyrite-rich chimney with a thin sphalerite and iron-oxide-rich exterior wall.
132625	Chalcopyrite–sphalerite zoned chimney with an iron oxide exterior.
132974	Sphalerite–barite-rich flange-type chimney piece with an iron oxide exterior.
132982	Sphalerite–pyrite-rich chimney with an iron oxide exterior.
133990	Fe-oxide crust.
134067-1	Sphalerite – barite – iron oxide-rich exterior piece of chimney.
134067-2	Sphalerite–barite-rich interior piece of chimney.
134228	Chalcopyrite-rich piece of chimney with a small orifice.
134237	Chalcopyrite-rich piece of chimney.
134238	Zoned chalcopyrite – sphalerite – iron oxide piece of chimney.

Snowcap

305-S-01	Top of a dead chimney, with a massive sphalerite, anhydrite interior and an iron oxide – manganese oxide exterior.
118303	Piece of pyrite–covellite–bornite-rich mushroom-shaped chimney.
118303A	Exterior piece of mushroom-shaped chimney.
118310	Iron–manganese oxide crust on altered hyaloclastite.
132381	Piece of sphalerite-rich chimney flange with thin iron oxide exterior.
132382	Sphalerite-rich piece of chimney, with minor iron oxide.
132400	Sphalerite – iron oxide-rich piece of chimney. Sphalerite lines a clogged orifice.
132497	Hyaloclastite composed of volcanic fragments 2 to 5 mm across cemented by very fine-grained pyrite.
132603	Hyaloclastite cemented by pyrite, minor native sulfur.
134078	Iron-oxide-rich mound sample.
134092	Iron-oxide-rich mound sample.
134191	Manganese-rich piece of hydrothermal crust.
134192	Manganese-rich piece of hydrothermal crust.

South Su

133832	Pyrite–bornite-rich crust.
133834	Pyrite-rich hyaloclastite.

Nimab

132689	Sulfidic mud.

TABLE 2. SUMMARY OF THE COMPOSITION OF HYDROTHERMAL PRECIPITATES, EASTERN MANUS BASIN

Vent site	SM	SC	R	RR	S	SC	RR	SM	RR	S	SM	RR	S	NS	SM	SC	R	SS	RR	N
Type	Sphalerite–barite					Sp–Gn		Sp–Ccp			Chalcopyrite				Sulfide-poor					
n	17	3	10	20	1	1	1	3	10	1	4	6	3	2	2	7	8	2	1	1
SiO_2 wt.%	2.41	8.10	5.10	2.80	1.01	2.66	0.35	0.08	7.15	1.37	0.54	5.68	3.54	1.51	0.18	13.69	62.25	25.06	37.63	75.28
CaO	0.11	0.05	0.14	0.11	0.46	0.07	0.09	0.09	0.10	0.16	8.19	0.07	0.73	0.08	37.59	0.61	0.37	0.16	0.54	0.28
Fe_2O_3	8.87	0.91	3.76	15.08	19.56	0.07	14.66	35.75	22.98	23.65	38.92	38.18	36.64	34.21	4.00	23.58	13.03	32.74	40.78	9.67
Na_2O	0.47	0.19	0.52	0.76	1.28	0.34	0.78	0.25	0.87	0.34	0.16	0.13	0.28	1.14	0.02	3.30	2.46	0.56	2.97	3.58
Cu	2.79	1.10	0.55	3.88	3.93	0.09	1.20	10.00	16.89	8.21	25.14	28.51	26.98	13.59	0.45	0.11	0.04	1.57	0.01	0.02
Zn	37.53	48.33	35.24	32.30	6.45	48.00	21.30	9.92	22.31	3.46	2.31	3.96	0.54	0.24	0.05	0.10	0.39	0.04	0.09	0.15
Pb	1.92	2.05	1.36	2.37	1.14	17.62	8.17	1.08	1.47	0.55	0.09	0.28	0.09	0.02	0.01	0.05	0.11	0.04	0.05	0.20
Ba	11.45	3.60	19.54	7.84	26.64	2.20	13.65	6.67	1.73	23.22	0.15	0.65	5.13	5.44	0.29	0.03	1.11	0.18	0.15	0.25
S	26.75	25.50	24.16	31.58	25.6	28.1	30.1	41.40	31.77	27.40	37.40	32.60	31.10	35.80	na	7.62	0.78	40.70	0.20	0.40
Mo ppm	15	18	6	51	149	4	58	46	108	148	159	285	206	3	8	346	186	12	21	23
Hg	17	42	13	8	43	2	59	12	7	18	10	8	4	30	1	1	2	18	1	1
Au	16.58	0.06	2.27	21.18	20.49	0.04	13.05	10.50	22.82	23.90	8.12	6.72	25.54	5.51	0.12	0.41	0.10	0.44	0.12	0.03
Ag	283	975	509	352	296	924	2031	49	282	211	72	86	102	38	1	12	5	33	1	2
As	7558	3359	4333	5451	7139	11956	4167	8093	6668	2386	1899	1795	722	43481	31	589	1682	5640	3262	1507
Sb	1049	296	720	842	1092	100	2978	370	931	426	208	216	116	841	1	13	95	206	27	112
Cd	1354	1644	1401	1521	664	1032	619	166	1089	278	81	213	38	17	2	6	10	17	6	4
Co	2	4	2	1	52	2	1	58	2	107	38	2	162	5	85	3	3	6	1	na
Bi	12	1	<1	<1	1	<1	<1	29	11	<1	42	<1	93	1	9	1	<1	4	<1	<1
Ge	59	11	8	20	1	11	6	8	39	1	1	8	1	2	na	2	3	4	3	1
Se	2	2	<1	6	5	<1	1	92	13	4	107	26	66	56	20	1	1	38	<1	<1
Te	2	1	1	2	1	<1	1	26	6	4	47	17	24	53	18	3	1	25	<1	1

Abbreviations: SM Satanic Mills, RR Roman Ruins, R Rogers Ruins, SC Snowcap, S Suzette, SS South Su, NS north Su, N Nimab, na not analyzed, n: number of samples, Sp sphalerite, Gn galena, Ccp chalcopyrite. Sample types are described in the text. Descriptions of individual samples are given in Table 1.

PACMANUS typically contain little gold (Fig. 3b). Similarly, iron–manganese oxide crusts and mounds and iron oxide chimneys are gold-poor. The sphalerite – barite-rich, predominantly inactive chimneys from the Roman Ruins vent sites are enriched in gold, as are the zoned chalcopyrite–sphalerite chimneys from the Satanic Mills and Susu Knolls areas. Massive chalcopyrite-rich chimneys, or chalcopyrite-rich portions, are variably enriched in gold, with one sample from the Susu Knolls area having the highest gold content encountered, 56.8 ppm (Fig. 3b). The concentration of gold shows statistically significant (at the 95% confidence level) positive correlations with that of Zn, Cu, S, Sb and Cd, (Figs. 4a–e). A significant negative correlation of Au with SiO_2 (Fig. 4g) is consistent with the low gold content of sulfide-poor samples in the area.

There is no unique position of gold enrichment within zoned chimneys from eastern Manus Basin, as both interior (Cu-rich) and exterior (Zn-rich) chimney portions contain high (>1 ppm) values of gold (Fig. 5). However, zinc-rich portions generally have the higher gold contents. One complexly zoned chimney selected for detailed analysis has a broad zone of gold enrichment in the Zn-rich middle chimney wall (Fig. 6). Analysis of sub-samples from a zoned chimney from Lau Basin produced a similar result (Herzig *et al.* 1993).

Mineralogy of Hydrothermal Precipitates

Sphalerite + barite samples

These samples consist predominantly of porous aggregates of sphalerite and prismatic crystals of barite that fill cavities in the sphalerite. Rosettes of barite are commonly intergrown with granular sphalerite, which may also be present as dendrites. In some places, there has been small-scale replacement of barite by sphalerite. Sphalerite contains most of the other sulfides encountered as inclusions or as cavity fill. Dendritic sphalerite contains predominantly pyrite inclusions, whereas granular sphalerite contains mostly chalcopyrite and tennantite inclusions.

Chalcopyrite forms fine (1–5 μm thick) "ribbons" outlining growth zones in sphalerite aggregates. Such zones are also outlined in places by tennantite and a Pb–As sulfosalt with the composition of dufrénoysite ($Pb_2As_2S_5$). Euhedral to subhedral grains of tennantite are associated with sphalerite, commonly forming a cavity-lining on sphalerite aggregates, and in some places replacing sphalerite inward from the cavities (Fig. 7a). Euhedral, triangular-shaped grains of tennantite up to 40 μm in diameter occur as inclusions in sphalerite.

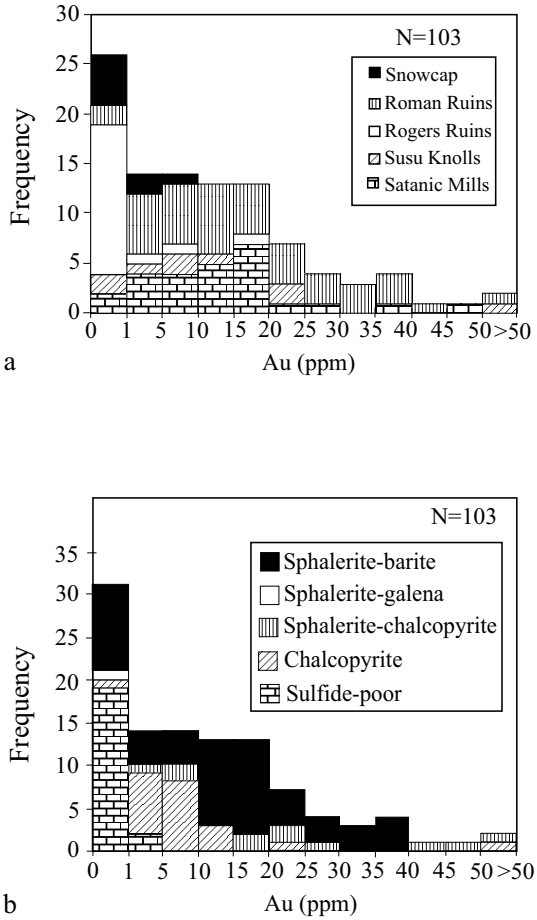

FIG. 3. Frequency distributions of gold content of hydrothermal precipitates. a. Distribution arranged by vent site. b. Distribution arranged by mineralogical composition of the precipitates. See text for description of mineralogical types.

Dufrénoysite is found predominantly as micrometric disseminations within sphalerite (Fig. 7b).

Spheroidal grains of pyrite up to 50 μm across or aggregates of spheroidal pyrite are associated with dendritic sphalerite. In some cases, marcasite replaces pyrite, as grains radially oriented toward the core of the spheroidal pyrite. Rare bornite and covellite are associated with chalcopyrite in the chimney interior.

(*Sphalerite + galena*)-*enriched samples*

This mineralogical type is represented by only two samples, recovered from the Snowcap and Roman Ruins vent sites at PACMANUS. Sphalerite occurs both as dendritic aggregates and as porous granular aggregates that appear to have formed by continuous precipitation on this dendritic framework. Galena is present as subhedral to anhedral grains of 10–50 μm diameter that rim and replace sphalerite, and as minor dendritic grains generally interstitial to sphalerite. Chalcopyrite, dufrénoysite, and tennantite occur as fine-grained (1–5 μm) inclusions in sphalerite. Tennantite may replace galena in places (Fig. 7c). Rare grains of pyrite are interstitial to sphalerite.

(*Sphalerite + chalcopyrite*)-*rich samples*

Mineralogically zoned chimneys, typically with a chalcopyrite-rich interior and sphalerite-rich exterior, comprise this type of sample. Chalcopyrite in the chimney interior occurs as both dendritic grains and massive aggregates that are porous in places. Exsolution lamellae of chalcopyrite, showing a typical basket-weave texture, occur in bornite in some samples (Fig. 7d). Later chalcopyrite replaces this bornite–chalcopyrite assemblage in places. Covellite is always associated with bornite, generally forming a rim around bornite grains, and replacing bornite along fractures and grain boundaries. Sphalerite lines cavities in the chalcopyrite and forms a thin (1–5 μm) rim around chalcopyrite aggregates. In some places, sphalerite also occurs as ribbon-like aggregates in chalcopyrite outlining growth zones or grain boundaries. Marcasite is common in chalcopyrite-rich zones, and occurs together with pyrite as very fine-grained intergrowths rimmed by chalcopyrite, and as grains and granular aggregates included in, and locally replaced by, chalcopyrite. Pyrite also occurs within chalcopyrite as euhedral to subhedral inclusions and interstitial grains. Minor barite may also occur in chimney interiors as large (up to 0.5 mm) bladed grains in the cavities of chalcopyrite aggregates.

The mineralogy in the middle to outer chimney wall is dominated by massive aggregates of sphalerite that are commonly colloform and banded. The growth zones are outlined by tennantite, dufrénoysite and, more rarely, chalcopyrite. The sphalerite typically becomes more dendritic toward the outer wall of the chimneys. Chalcopyrite occurs as inclusions in sphalerite, or lines cavities in sphalerite aggregates. Tennantite and a later generation of sphalerite commonly form rims on this chalcopyrite which, in some places, replaces the earlier sphalerite. Rosettes of barite are found only in the outer portions of chimneys, typically concentrated right at the exterior wall.

Chalcopyrite-rich samples

Although some samples from the Satanic Mills vent site are chalcopyrite-rich, most samples of this type come from the Suzette vent site in the Susu Knolls area. Massive aggregates of chalcopyrite dominate, and commonly have a thin (20 μm) rim of sphalerite, which also outlines grain boundaries within the chalcopyrite. Isolated grains of chalcopyrite (up to 20 μm) occur around

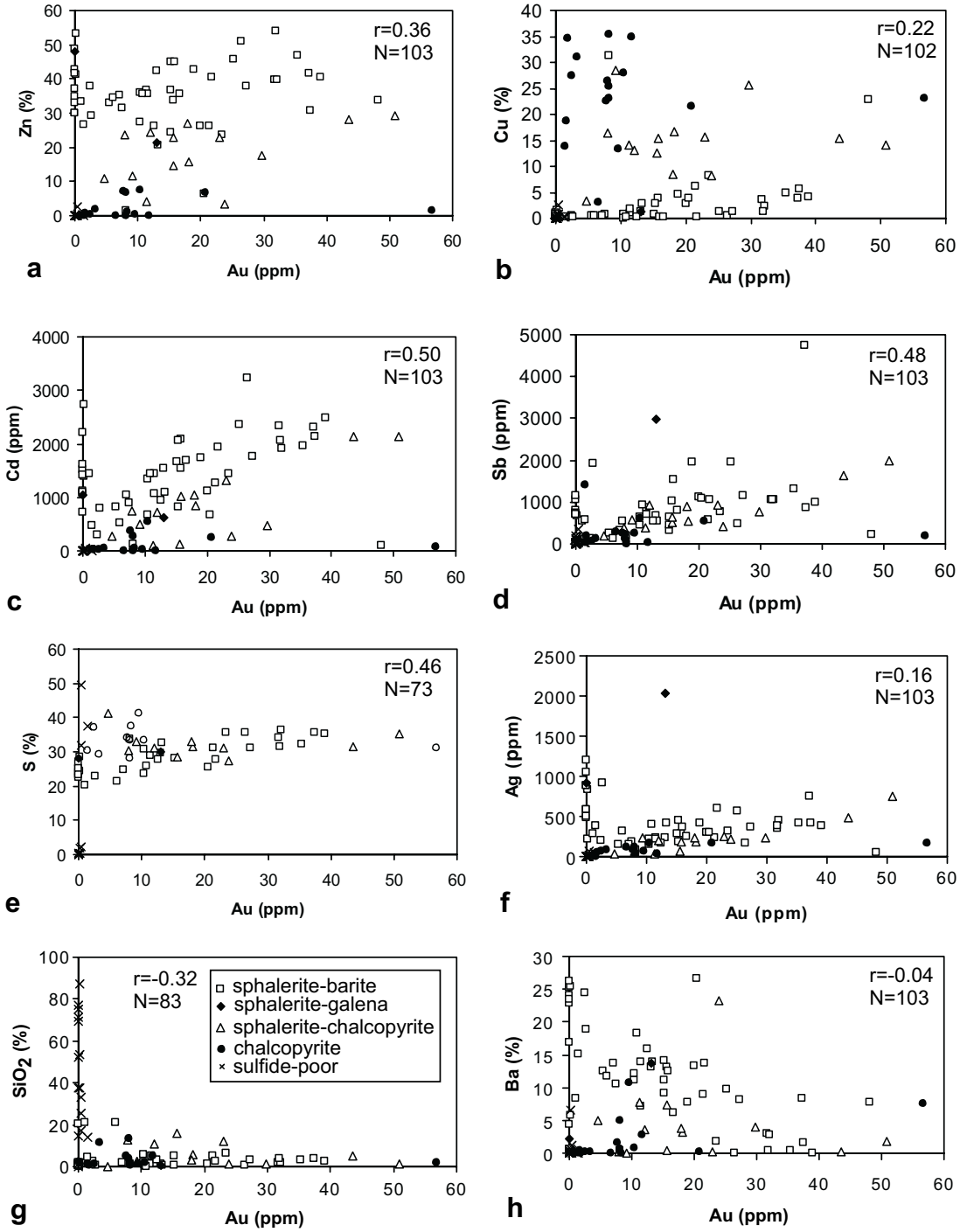

FIG. 4. Scatterplots of gold *versus* a) Zn, b) Cu, c) Cd, d) Sb, e) S, f) Ag, g) SiO_2, h) Ba.

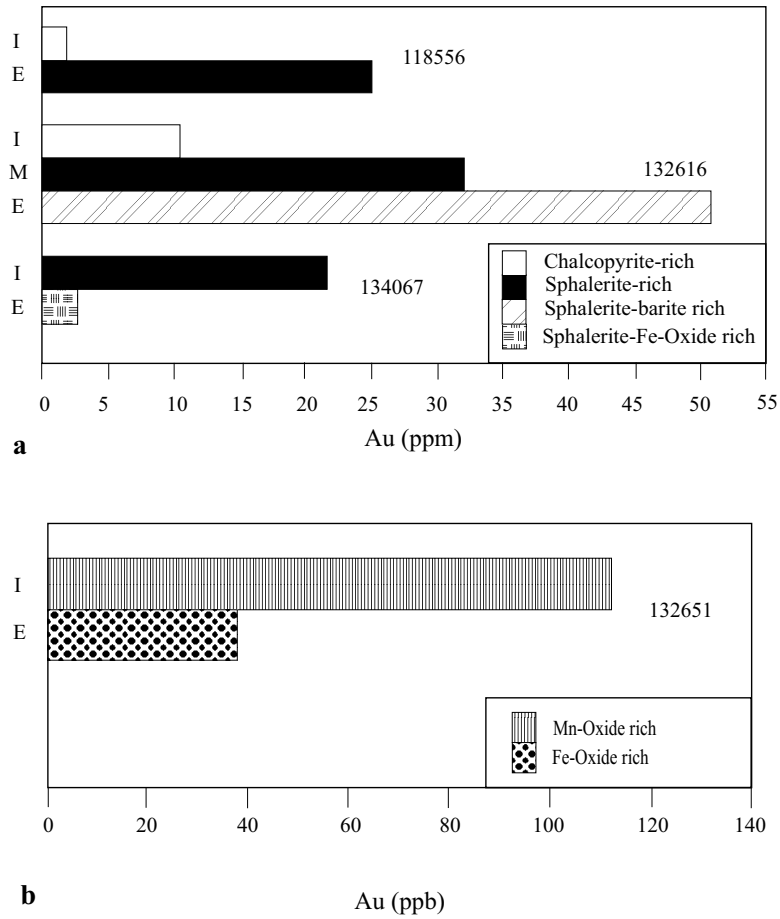

FIG. 5. Gold content of selected zoned chimneys from the PACMANUS vent field. a. Sulfide-rich chimneys. b. Oxide-rich chimneys. Note change of units (to ppb) in b. Numbers to the right of the bars are sample numbers. Abbreviations: I interior, M middle, E exterior chimney wall.

sphalerite rims in places, suggesting rapidly changing conditions in the fluid, with alternating precipitation of chalcopyrite and sphalerite. Tennantite is associated with the chalcopyrite–sphalerite assemblage as rare grains that separate chalcopyrite and sphalerite. Marcasite and pyrite are also associated with the massive chalcopyrite, mostly as pyrite–marcasite aggregates in which pyrite has been variably replaced by marcasite. Bornite fills cracks in the chalcopyrite aggregates, and may replace chalcopyrite inward from grain boundaries and cavities (Fig. 7e). Covellite replaces bornite along fractures in places (Fig. 7f), but also occurs as euhedral grains rimming chalcopyrite. The exterior walls of copper-rich chimneys contain minor barite, iron oxides and, rarely, atacamite [$Cu_2Cl(OH)_3$].

Sulfide-poor samples

Sulfide-poor samples from the eastern Manus Basin fall into three groups: 1) iron–manganese oxides predominantly composed of goethite, ferrihydrite, hematite and Mn-oxide hydrate ($Mn_7O_{13}\cdot 5H_2O$), 2) sulfate-rich samples dominated by barite or, more rarely, anhydrite, with lesser gypsum, and 3) silicate-rich samples that are composed mostly of amorphous silica and rare kaolinite.

Occurrences of gold in sulfides at Manus

A total of 303 grains of native gold were observed in four samples of hydrothermal precipitates from Eastern

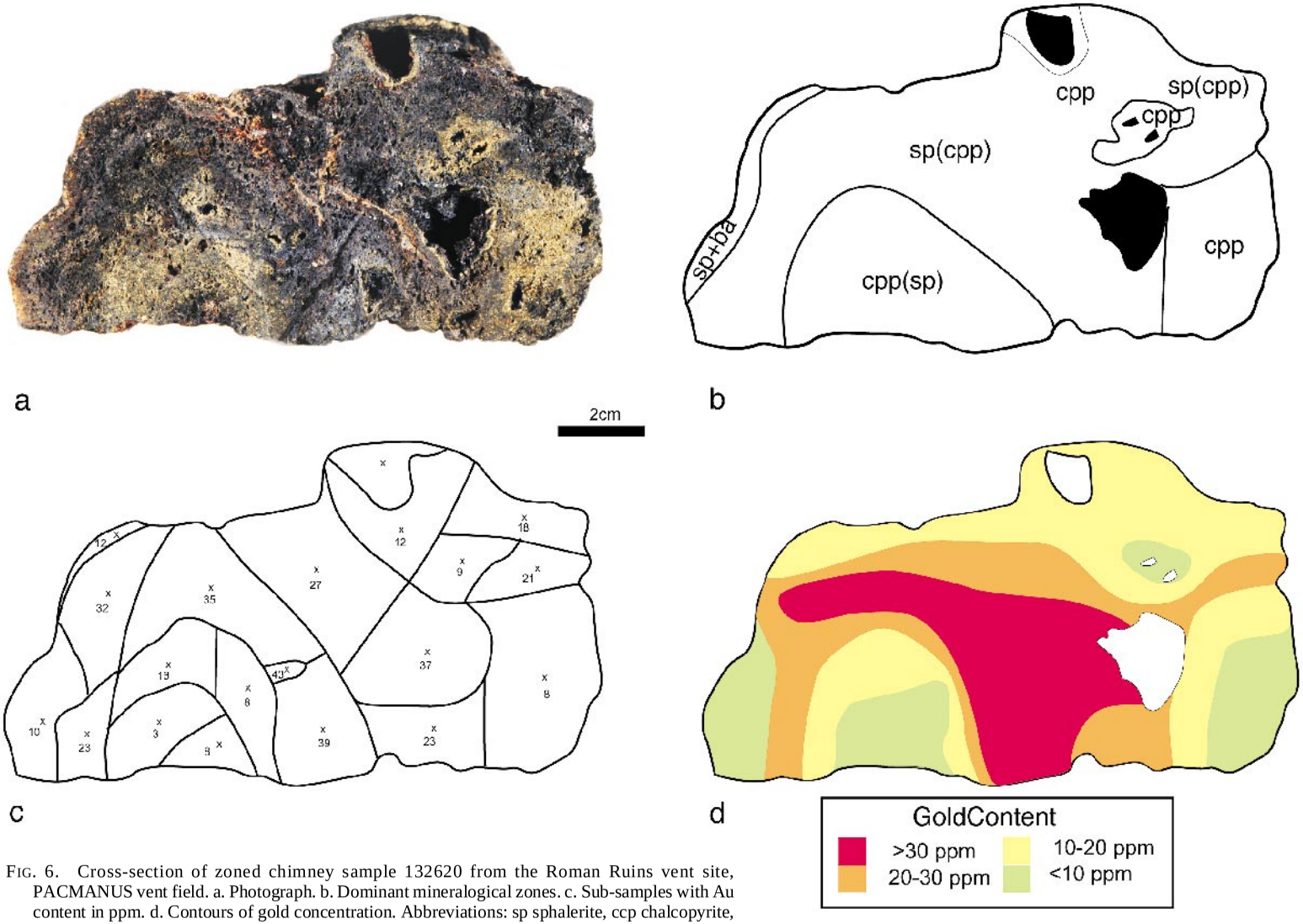

FIG. 6. Cross-section of zoned chimney sample 132620 from the Roman Ruins vent site, PACMANUS vent field. a. Photograph. b. Dominant mineralogical zones. c. Sub-samples with Au content in ppm. d. Contours of gold concentration. Abbreviations: sp sphalerite, ccp chalcopyrite, ba barite. Mineral in parentheses is a minor constituent of the zone.

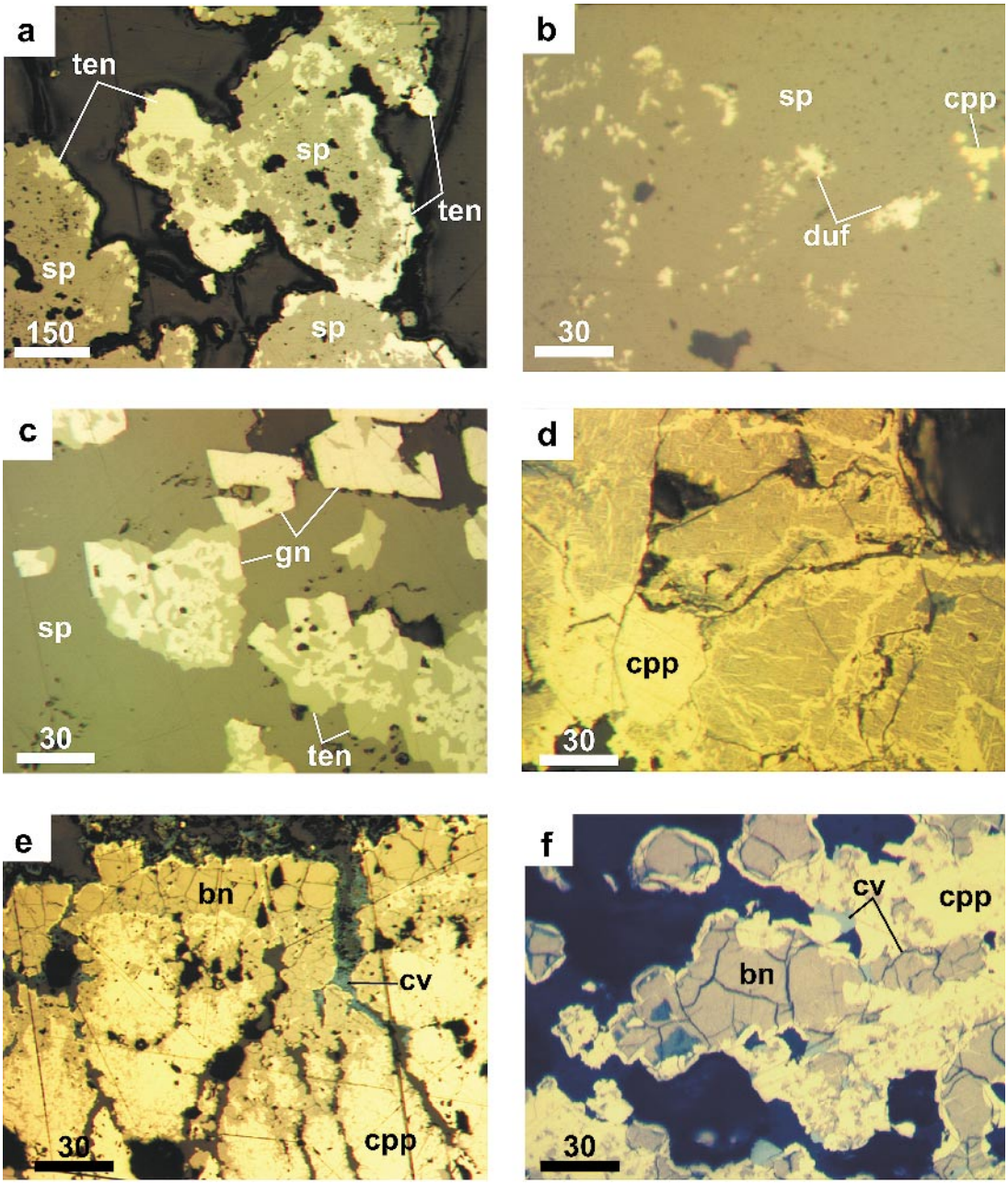

FIG. 7. Reflected-light photomicrographs of hydrothermal precipitates from the eastern Manus Basin. a. Sphalerite + barite sample. Tennantite (ten) rims massive sphalerite (sp). b. Sphalerite + barite sample. Dufrénoysite inclusions (duf) in massive sphalerite (sp). c. Sphalerite + galena ± barite sample. Replacement of galena (gn) by tennantite (ten) in massive sphalerite (sp). d. Sphalerite – chalcopyrite sample. Exsolution lamellae of chalcopyrite (ccp) in bornite and replacement of this assemblage by chalcopyrite. e. Chalcopyrite-rich sample. Replacement of chalcopyrite (cpp) by bornite (bn) inward from a cavity located at the top of the photo. Bornite is replaced along grain boundaries by covellite (cv). f. Chalcopyrite-rich sample. Replacement of bornite (bn) by covellite (cv) along fractures and grain boundaries. Chalcopyite (cpp) rims bornite grains and lines cavities in the bornite. It also replaces bornite inward from cavities. Scales are in micrometers.

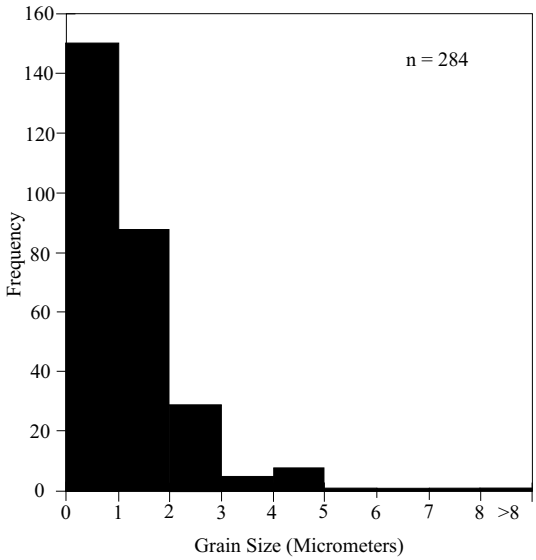

FIG. 8. Grain-size distribution of grains of native gold in sulfide chimneys from the PACMANUS and Susu Knolls vent sites.

Manus Basin. The grains are typically roundish and small; 75% of the grains are less than 3 μm in diameter (Fig. 8). The main occurrence of gold grains is as inclusions in tennantite (77% of grains found), followed by inclusions in chalcopyrite (16%). The remainder occur as inclusions in sphalerite or bornite, fracture fill in various sulfides, and are found as isolated grains along grain boundaries and in cavities (Table 3).

Gold grains were found in a (sphalerite + barite)-rich sample, two (sphalerite + chalcopyrite)-rich samples and in a chalcopyrite-rich sample. In the (sphalerite + barite)-rich sample, the grains are associated with a chalcopyrite – sphalerite – tennantite assemblage and occur mostly as inclusions in tennantite or chalcopyrite aggregates (Fig. 9a). Gold grains in chalcopyrite tend to occur close to grain boundaries with tennantite. Inclusions of tennantite also occur in sphalerite, but these inclusions do not contain grains of gold. Gold therefore occupies a very specific position in the mineral paragenesis, occurring as part of late-stage cavity-filling episodes, together with tennantite and sphalerite that lines the walls of cavities in chalcopyrite (Fig. 9b). All of the gold in this assemblage was precipitated prior to sphalerite, however, as no gold grains are visible in the sphalerite, nor in the tennantite inclusions in sphalerite.

Gold grains in chalcopyrite-rich sample 133012 from the Suzette vent site are mostly present as inclusions in chalcopyrite (Fig. 9c). Although bornite and rare covellite also form part of this assemblage, primarily replacing chalcopyrite, only one grain of gold was found associated with bornite (Table 3). The association of gold primarily with chalcopyrite indicates that it formed prior to replacement of chalcopyrite by bornite and covellite.

The interior chimney wall of zoned (sphalerite + chalcopyrite)-rich sample 132376 contains grains of gold associated with a bornite – chalcopyrite – tennantite assemblage (Fig. 9d). Gold occurs mainly as inclusions in, or as grains interstitial to, tennantite and chalcopyrite that is later than the bornite – chalcopyrite – covellite assemblage.

All of the grains of gold are silver-poor. Electron-microprobe analyses of several grains from samples 118554–6 [(sphalerite + barite)-rich] and 132376 (chalcopyrite-rich) average 4 ± 0.15 wt.% and 1.9 ± 0.3 wt.% Ag, respectively (Table 4). Gold grains of similar low content of Ag are associated with Fe-poor sphalerite in sulfides in the Lau Basin (Herzig *et al.* 1993). Although there is a slight decrease in silver content of gold in the Cu-rich samples over that in the Zn-rich samples, this is very much less than that observed by Huston *et al.* (1992) for gold in Australian volcanogenic massive sulfide deposits.

TABLE 3. MODE OF OCCURRENCE OF GOLD GRAINS IN MANUS BASIN SULFIDES

Inclusions in	chalcopyrite	49
	tennantite	232
	sphalerite	5
	bornite	1
Fractures in minerals		5
Grain boundaries		7
Cavity fill		4
Total		303

TABLE 4. COMPOSITION OF GOLD GRAINS IN EASTERN MANUS BASIN SULFIDES

Sample No.	Au wt.%	Ag wt.%	Total[1]	Fineness[2]
118554-6-3	101.20	4.24	105.44	960
118554-6-6	100.20	3.88	104.08	963
118554-6-8	98.73	3.97	102.70	961
118554-6-11	95.05	4.04	99.09	959
132376-3-6	102.33	1.58	103.91	985
132376-3-7	90.49	2.06	92.55	978
132376-3-8	99.16	2.06	101.22	980
132376-3-9	98.54	1.39	99.93	986
132376-3-10	101.68	2.00	103.68	981
132376-3-11	104.73	1.92	106.65	982
132376-3-11(2)	101.56	1.56	103.12	985
132376-3-12	101.60	2.49	104.09	976
132376-3-13	91.49	1.80	93.29	981
132376-3-14	102.25	1.96	104.21	981

[1] High totals are a result of the difficulty in analyzing the very small grains of gold, 98% of which are less than 5 μm in diameter. The small grain-size results in fluorescence of the surrounding material (typically chalcopyrite or tennantite), despite using low beam-currents. [2] Fineness = 1000 Au/(Au + Ag).

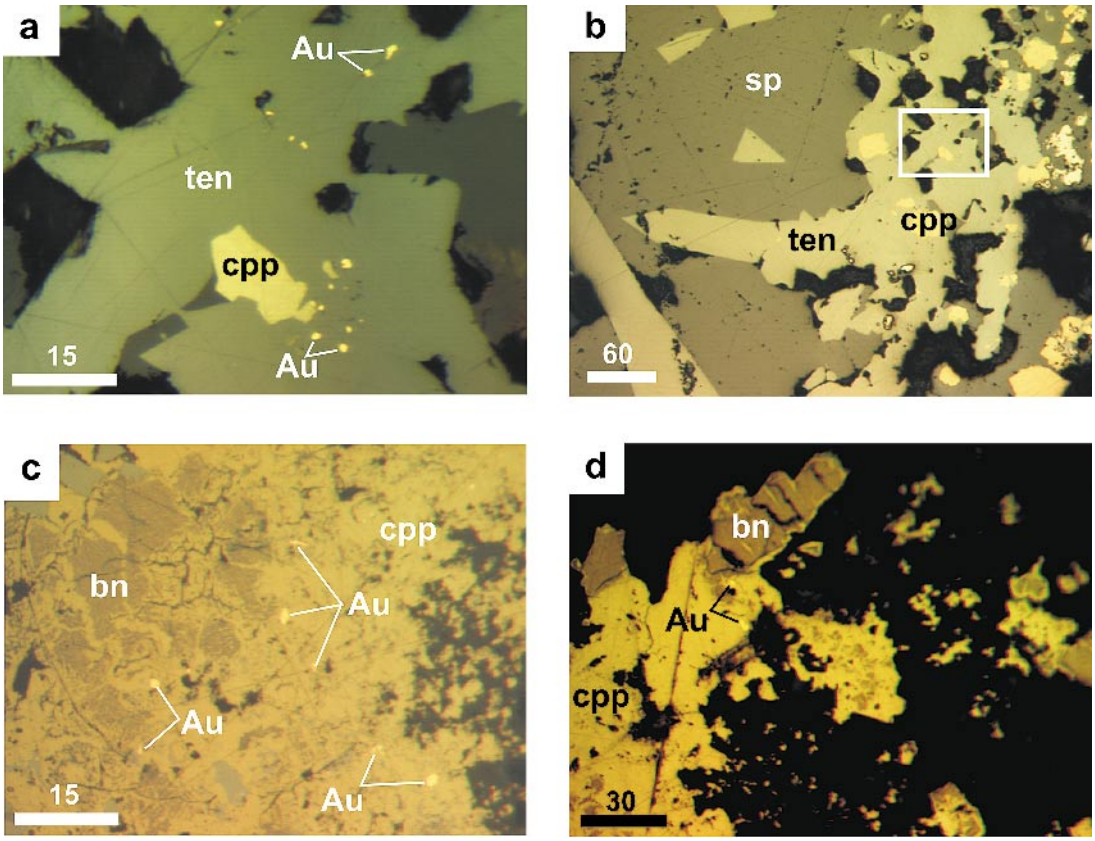

FIG. 9. Photomicrographs of native gold and associated assemblages. a. (Sphalerite + barite)-rich sample. Several inclusions of native gold (Au) in tennantite (ten) are associated with sphalerite (sp) in a cavity lining. b. Gold – tennantite – chalcopyrite – sphalerite association. Box indicates position of photomicrograph in a. The native gold occurs mainly in the tennantite (ten) that forms a rim on the chalcopyrite (cpp), but a few grains also are present in the chalcopyrite. Triangular inclusions of tennantite in sphalerite (sp) do not contain visible grains of gold. c. Zoned sphalerite–chalcopyrite-rich sample. Gold – chalcopyrite – bornite association. Gold (Au) occurs mainly in the massive chalcopyrite (cpp) aggregates, and only rarely as inclusions in bornite (bn). d. Chalcopyrite-rich sample. Gold is typically associated with chalcopyrite (cpp), which is later than the chalcopyrite–bornite exsolution assemblage. Scales are in micrometers.

Gold is known to occur as submicroscopic grains, so-called "invisible" gold (Cook & Chryssoulis 1990). This may be structurally bound gold in common sulfides such as pyrite and chalcopyrite, fine-grained gold adsorbed onto mineral surfaces, or very fine-grained (colloidal) gold in sulfide grains. The presence of such submicroscopic gold in the PACMANUS sulfides would explain the absence of grains of native gold from some samples having high bulk-gold contents, as suggested by Hannington *et al.* (1995) for gold in the TAG precipitates. The significant positive correlation of gold with Zn, Cd, and S in the PACMANUS sulfides (Fig. 4) and the lack of such a correlation with Ag or As suggest that although the microscopically visible gold occurs in association with tennantite and chalcopyrite, a significant proportion of the gold at PACMANUS is present as "invisible" gold in sphalerite. Attempts to determine the amount of gold in the sphalerite by secondary-ion mass spectroscopy were unsuccessful owing to the very fine-grained nature of the sphalerite.

DISCUSSION

Mineralogical associations of native gold

There are three mineralogical associations of gold in eastern Manus Basin sulfides: a chalcopyrite – sphalerite – tennantite association, a chalcopyrite – bornite ± covellite association and a chalcopyrite – tennantite ± bornite – covellite association. Native gold

occurs predominantly as micrometric inclusions in tennantite and chalcopyrite. The chalcopyrite – sphalerite – tennantite association is present in the (sphalerite + barite)-rich chimneys. Similar occurrences of native gold have been described from other seafloor vent-sites (*e.g.*, Hannington & Scott 1989a, b, Herzig *et al.* 1993), but in most of these cases the host is Fe-poor sphalerite with associated tetrahedrite or tennantite. Native gold and a gold–silver alloy ("electrum") have also been reported from zinc-rich assemblages in ancient deposits. Australian volcanogenic massive sulfide deposits of the Zn–Pb–Ag–Au type typically contain "electrum" associated with galena, sphalerite, chalcopyrite and tetrahedrite–tennantite (Huston *et al.* 1992), as do deposits of the Rio Tinto – Aznalcollar–La Zarza type of the Iberian Pyrite Belt (Leistel *et al.* 1998). The association of native gold with low-temperature (<300°C) Zn-rich precipitates is commonly believed to be due to the transport of gold predominantly as the $Au(HS)_2^-$ complex (*e.g.*, Hannington & Scott 1989a, b, Huston & Large 1989).

Gold–copper associations, such as the gold – chalcopyrite – bornite ± covellite assemblage found in copper-rich chimneys at Suzette, are rare in seafloor sulfide deposits. Gossans developed on the TAG and MIR hydrothermal mounds on the Mid-Atlantic Ridge have an average gold content of 11.4 ppm and contain abundant grains of native gold associated with covellite, digenite, native copper and atacamite (Hannington *et al.* 1988). However, these copper minerals at TAG are secondary, resulting from oxidation processes on the seafloor (Hannington *et al.* 1988, Herzig *et al.* 1993), and are not comparable to the primary association found in eastern Manus Basin. A gold–copper association occurs in the ultramafic-rock-hosted Logatchev hydrothermal field at 14°45' N on the Mid-Atlantic Ridge (Murphy & Meyer 1998). Here, gold mineralization is found both as primary grains of native gold included in chalcopyrite associated with sphalerite and isocubanite, and as secondary gold associated with a chalcopyrite – bornite – covellite assemblage. Occurrences of gold–copper associations have been well documented in ancient volcanogenic massive sulfide deposits (Huston & Large 1989, Large 1990, Huston *et al.* 1992, Leistel *et al.* 1998). Such associations have been interpreted as resulting from chloride complexing of gold in high-temperature (>300°C) fluids with precipitation due, in most part, to decreasing temperature (*e.g.*, Huston & Large 1989).

Effect of sulfur activity on gold concentration

The assemblages of sulfide minerals observed in Manus Basin, such as tennantite, chalcopyrite, bornite and pyrite, indicate a high activity of sulfur for sample types containing native gold. Also, electron-microprobe analyses of 68 sphalerite grains and aggregates from 13 PACMANUS samples have a low average iron content, 2.3 ± 3.1 mole % FeS (Fig. 10a), implying a high activity of sulfur. The low silver content of the gold grains in eastern Manus Basin also indicates a high activity of sulfur. The silver content of "electrum" in equilibrium with Ag_2S (or another Ag-bearing phase) is inversely proportional to the activity of sulfur (Barton & Toulmin 1964), as shown in equation 1.

$$Ag_{(s)} + \tfrac{1}{4}S_{2(g)} = \tfrac{1}{2}Ag_2S_{(s)} \qquad (1)$$
$$a_{Ag} = a_{Ag2S}^{1/2} \times a_{S2}^{-1/4} \times k^{-1}$$

The high activity of sulfur is consistent with the transport of gold as a reduced sulfur complex. There is no correlation of mole % FeS in sphalerite with the bulk-gold content of the PACMANUS samples (Fig. 10b), as was found to be the case with Tasmanian volcanogenic massive sulfide deposits (Zaw & Large 1996). However, when these parameters are plotted together with results from other seafloor vent-sites, the eastern Manus Basin data lie on a trend toward higher gold values with lower iron content of sphalerite (Fig. 11).

The concentration of gold in hydrothermal precipitates has been shown to be inversely related to the FeS content of sphalerite (Hannington & Scott 1989b). The FeS content of sphalerite coexisting with pyrite or pyrrhotite is known to be inversely related to the activity of sulfur (Barton & Toulmin 1966, Scott & Barnes 1971). Thus the gold content of seafloor sulfide deposits is related to the activity of sulfur, being generally highest where the activity of sulfur is highest (Hannington & Scott 1989b). This correlation is primarily due to the transport of gold as a sulfide complex in low-temperature (<300°C), reduced, sulfur-rich fluids that typically form gold-rich precipitates (Hannington & Scott 1989b). The Cambrian massive sulfide deposits in Tasmania also show a trend of increasing gold values with decreasing mole % FeS in sphalerite (Zaw & Large 1996). Although the correlation within an individual deposit is poor, it improves significantly if the values for each deposit are averaged and plotted as an individual point. Several reasons are put forth by Zaw & Large (1996) for this lack of correlation within a deposit, including later metamorphic effects, and factors other than sulfur activity and temperature controlling gold transport. Although it is clear that factors such as pH and oxygen activity play a role in transporting gold, inspection of relevant equations presented below indicates that the activity of reduced sulfur (in this case as H_2S) is the most important control on gold transport as a reduced sulfur complex.

Transport of gold in seafloor hydrothermal systems

Experimental studies of gold solubility have focused mainly on the ability of chloride and reduced sulfur ligands to complex gold, owing to their availability in hydrothermal systems (Seward 1991). There is a general consensus that gold is transported as the bisulfide

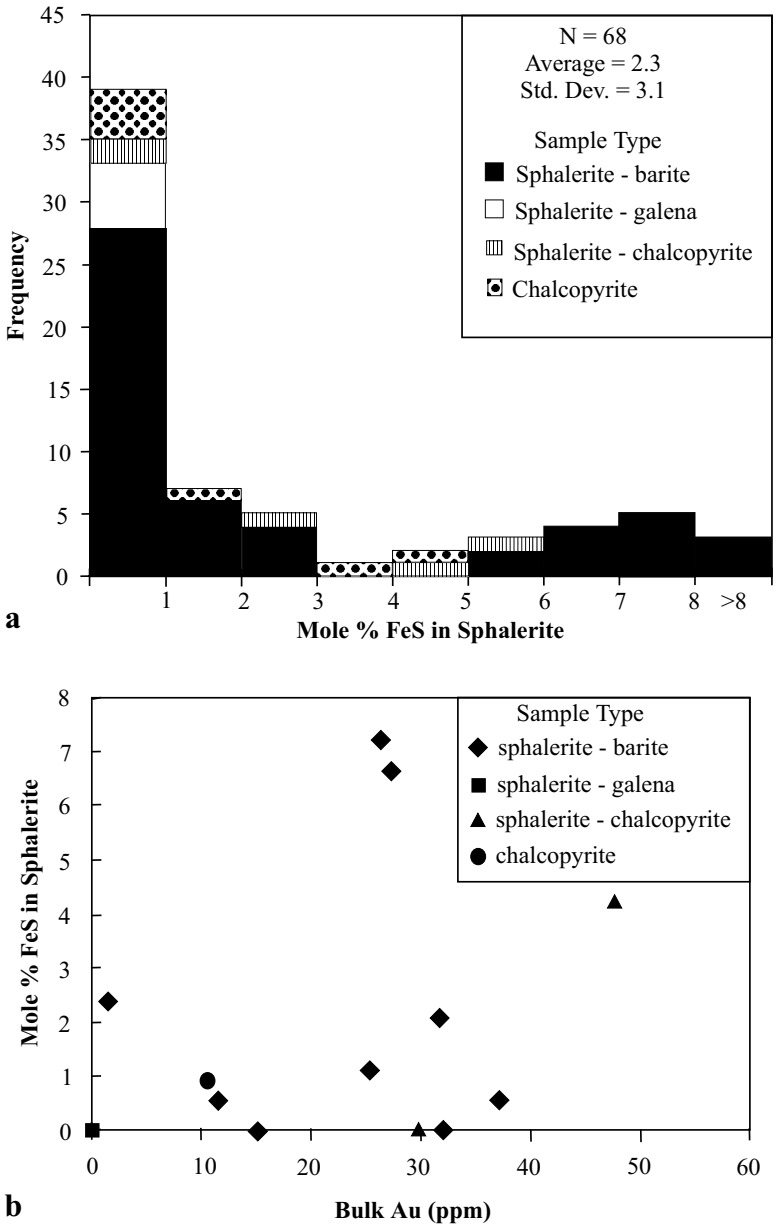

FIG. 10. a. Frequency distribution of mole % FeS in sphalerite in samples from the PACMANUS and Susu Knolls vent fields. b. Plot of average mole % FeS *versus* average gold content of the samples. See text for description of sample types.

$Au(HS)_2^-$ complex in fluids of low salinity, near-neutral pH, temperatures less than about 350°C and moderately reducing conditions (*e.g.*, Seward & Barnes 1997). For gold transport in fluids of low pH, low salinity and temperatures up to 350°C, Hayashi & Ohmoto (1991) proposed the $HAu(HS)_2°$ complex. However, recent experimental work has shown that the AuHS° complex is dominant under these conditions (Benning & Seward 1996).

Chloride complexing of gold has also been the source of some debate, as Cole & Drummond (1986) have suggested that the stability of the $AuCl_2^-$ complex

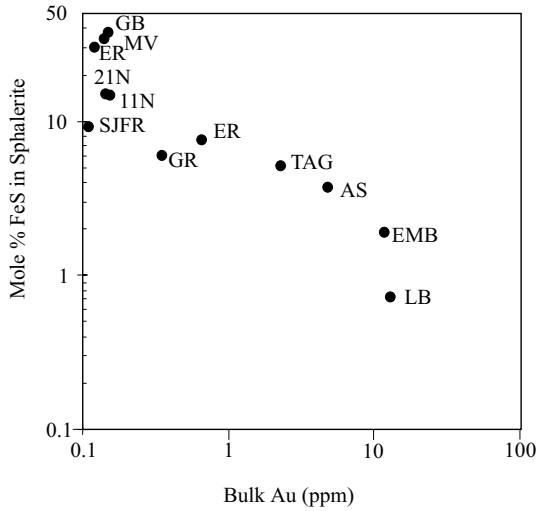

FIG. 11. Plot of average mole % FeS *versus* average gold content for seafloor VMS deposits. Abbreviations: GB Guaymas Basin, MV Middle Valley, ENR Endeavour Ridge, 21N 21°N East Pacific Rise, 11N 11°N East Pacific Rise, SJFR Southern Juan de Fuca Ridge, GR Galapagos Ridge, ER Explorer Ridge, AS Axial Seamount, EMB eastern Manus Basin, LB Lau Basin. Sources of data: Lau Basin: Herzig *et al.* (1993); eastern Manus Basin: this study; all other data: Hannington & Scott (1989b).

is far greater than that predicted by Helgeson (1969). However, Seward (1991) demonstrated that the data of Helgeson comprise part of a consistent dataset over the temperature range 25°C to 374°C. In addition, the experimental results of Zotov *et al.* (1991) and Gammons *et al.* (1994) have confirmed Helgeson's predicted solubilities. The solubility predicted by Sverjensky *et al.* (1997) and determined experimentally by Gammons & Williams-Jones (1995) is somewhat higher (Fig. 12). Sverjensky *et al.* (1997) also presented data for the AuCl and $AuCl_3^{2-}$ complexes, which are used in this study together with the solubility for the $AuCl_2^-$ complex predicted by Sverjensky *et al.* (1997) to evaluate gold transport as chloride complexes. The $Au(OH)^o$ complex may also play a role in gold transport at temperatures between 300° and 500°C (Gammons & Williams-Jones 1997).

Six complexes are therefore evaluated as possible carriers of gold in the hydrothermal systems of the eastern Manus Basin. Gold transport as a reduced sulfur complex may be represented by:

$$Au_{(s)} + 2H_2S_{(aq)} + \tfrac{1}{4}O_2 = Au(HS)_2^- + H^+ + \tfrac{1}{2}H_2O \quad (2)$$

or

$$Au_{(s)} + H_2S_{(aq)} + \tfrac{1}{4}O_2 = AuHS^\circ + \tfrac{1}{2}H_2O \quad (3)$$

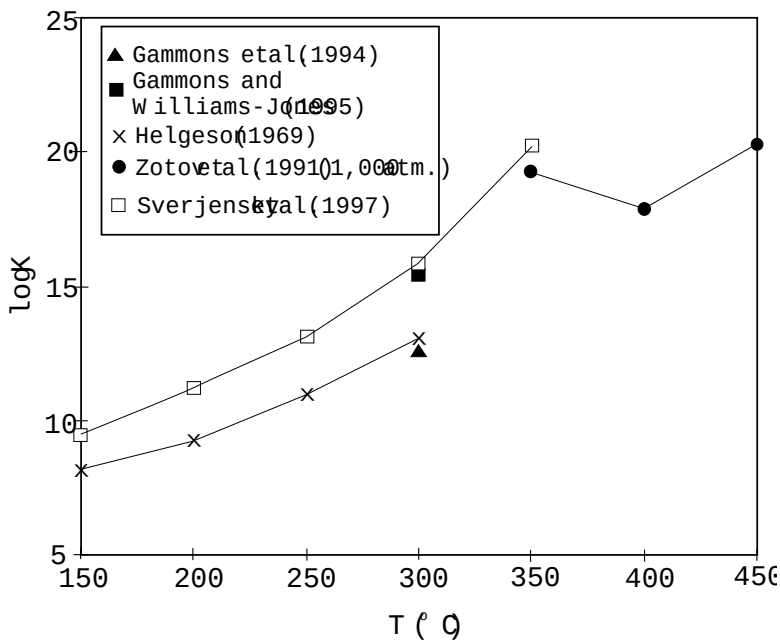

FIG. 12. Comparison of experimentally determined and calculated stabilities of the $AuCl_2^-$ complex (Equation 5).

chloride complexing of gold by:

$$Au_{(s)} + Cl^- + H^+ + \tfrac{1}{4}O_2 = AuCl^\circ + \tfrac{1}{2}H_2O \quad (4)$$

$$Au_{(s)} + 2Cl^- + H^+ + \tfrac{1}{4}O_2 = AuCl_2^- + \tfrac{1}{2}H_2O \quad (5)$$

$$Au_{(s)} + 3Cl^- + H^+ + \tfrac{1}{4}O_2 = AuCl_3^{2-} + \tfrac{1}{2}H_2O \quad (6)$$

and hydroxide complexing of gold by:

$$Au_{(s)} + \tfrac{1}{2}H_2O + \tfrac{1}{4}O_2 = Au(OH)^\circ \quad (7)$$

From equation 2, the solubility of gold as the $Au(HS)_2^-$ complex is primarily dependent on the activity of H_2S and pH and, to a lesser extent, on oxygen activity. Equation 3 indicates that the solubility of gold as the AuHS° complex is also primarily dependent on the activity of H_2S, but is independent of pH where H_2S is the stable sulfur species. From equations 4, 5 and 6, the stability of the gold chloride complexes is primarily dependent on the activity of chloride and pH and, to a lesser extent, on oxygen activity. Equation 7 indicates that gold carried as the Au(OH)° complex is predominantly dependent on oxygen activity.

The effect of pH on the chloride and sulfide complexes is shown for a PACMANUS-type vent fluid at 250°C in Figure 13a. The AuHS° complex is clearly the most stable in the acid pH region, but $Au(HS)_2^-$ becomes the most stable complex at pH greater than about 4.5. The gold chloride species $AuCl_2^-$ is more stable than the bisulfide species $Au(HS)_2^-$ (but much less stable than the AuHS° species) only in the very acid regions up to a pH of approximately 2. Thereafter, the bisulfide complex rapidly becomes the more stable of the two.

Temperature is also a key control on the complexing of gold, and is evaluated, for the PACMANUS-type fluid, at pH = 3, in Figure 13b. The sulfide complexes are clearly more stable than the chloride complexes up to close to 300°C, at which point the $AuCl_2^-$ species becomes more stable than the $Au(HS)_2^-$ species. However, even at this temperature, the concentration of the AuHS° species is two orders of magnitude greater than the chloride complex. Therefore, the bisulfide complex $Au(HS)_2^-$ is the most stable of the three complexes up to about 140°C, after which AuHS° becomes the stable complex up to 325°C. Calculations of gold solubility in the temperature range 300° to 400°C at 1 kbar indicate that the $AuHS^o$ complex remains the most stable of the complexes to a temperature of about 322°C. At this temperature, the neutral Au(OH)° complex becomes the most stable, and continues to be the dominant complex beyond 400°C (Fig. 13c).

The availability of suitable ligands to complex the gold plays a significant role in the transport of gold. A predominance-area diagram illustrating the fields of the complexes as a function of chloride and H_2S activity is shown in Figure 14. At very high activities of H_2S, the

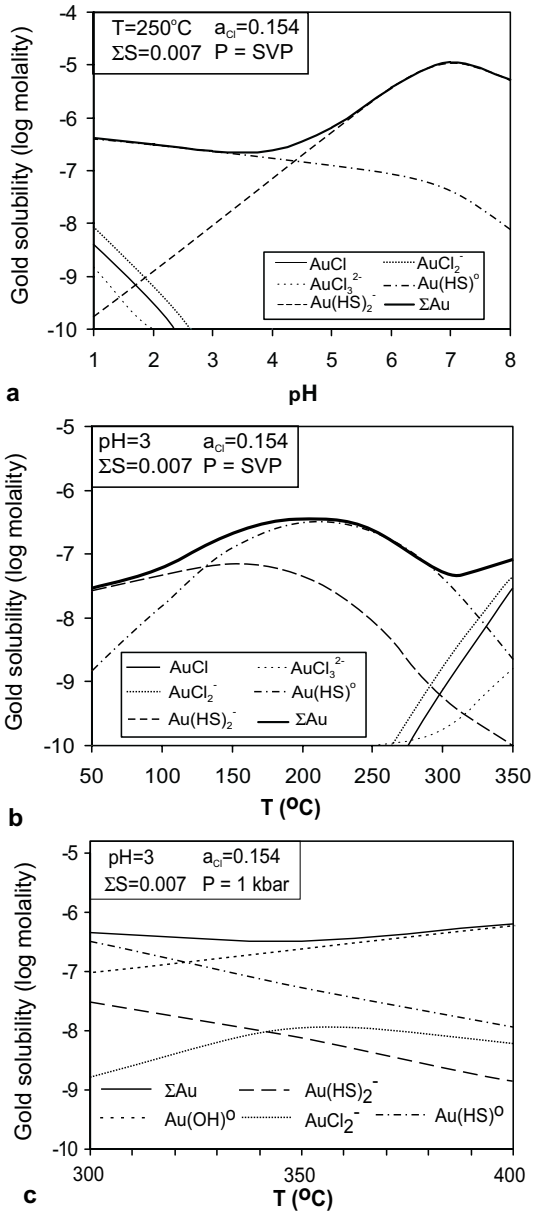

FIG. 13. Solubility of gold in a PACMANUS-like fluid a) as a function of pH, b) as a function of temperature, and c) for T between 300 and 400°C and P = 1 kbar. Gold acetate complexes have solubilities of < –10 log molal. Fluid composition is based on analyses of PACMANUS vent fluids (T. Gamo, pers. commun., 1995) extrapolated to 0 Mg, with activity of species and high-temperature pH calculated using SOLMINEQ.88 (Kharaka *et al.* 1988). Solubility was calculated using the EQBRM code (Anderson & Crerar 1993) with thermodynamic data from Benning & Seward (1996), Sverjensky *et al.* (1997), Suleimenov & Seward (1997), Johnson *et al.* (1992), and Zotov *et al.* (1985, 1991). SVP: saturated vapor pressure.

$Au(HS)_2^-$ complex is favored, and gold solubility can reach very high values. At lower activities of H_2S and low activity of chloride, gold is transported predominantly as the AuHS° complex, with a maximum solubility of 1.2 ppm Au. At sufficiently low values of H_2S activity and relatively high chloride activity, gold is transported predominantly as a chloride complex. The AuCl complex is only important at very low activities of H_2S [log $a(H_2S) < -6$] and low chloride activity. As the chloride activity increases, $AuCl_2^-$ becomes the predominant chloride complex, and finally at very high activity of chloride, $AuCl_3^{2-}$ is predominant. Average values of $a(H_2S)$ and $a(Cl^-)$ for the PACMANUS vent field indicate that gold in the PACMANUS system is most likely carried as the AuHS° complex, and has a maximum solubility of about 100 ppb (Fig. 14). Of course, the actual concentration of gold in the PACMANUS end-member fluid could be less than this value indicative of saturation.

Deposition of gold carried as the AuHS° complex can be caused by 1) a decrease in $a(H_2S)$ (see Fig. 14), which may result from dilution by ambient seawater, precipitation of sulfides, or phase separation with loss of H_2S to the vapor phase, 2) a change in pH (see Fig. 13a), and 3) sufficient oxidation to convert reduced sulfide to sulfate (Fig. 15). The effects of temperature on the solubility of gold are variable. At temperatures between approximately 322° and 200°C, gold solubility actually increases as temperature decreases owing to the predominance of bisulfide complexes (Fig. 13b). At lower temperatures, gold solubility decreases with the concentration of the gold bisulfide complexes. In the case of seafloor hydrothermal systems, such as PACMANUS, precipitation of gold from the hydrothermal fluid can be accomplished efficiently by mixing with seawater (Hannington & Scott 1989a). Such mixing causes a decrease in $a(H_2S)$ and an increase in pH and $a(O_2)$, all of which can result in precipitation of gold. Boiling may also be important in shallow submarine hydrothermal systems (Hannington *et al.* 1999). If boiling does occur, it will cause loss of H_2S to the gas phase prior to, or together with, mixing with seawater. This would result in more efficient precipitation of gold carried as a bisulfide complex than would mixing with seawater alone.

Conclusions

Gold-rich hydrothermal precipitates from the eastern Manus Basin are associated with both Zn- and Cu-

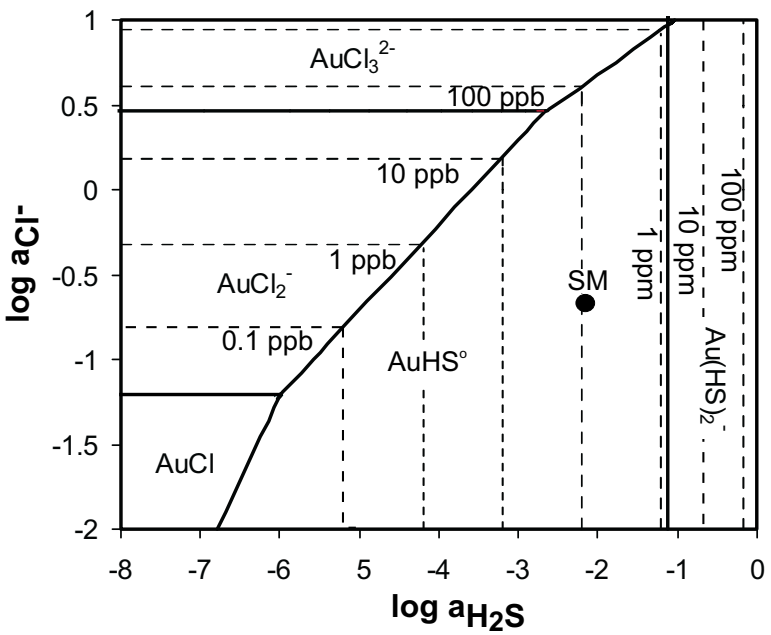

FIG. 14. Predominance-field diagram for selected complexes of gold, showing the position of the Satanic Mills (SM) vent fluid. T = 250°C, pH = 3, P = saturated vapor pressure. Contours are for gold solubility in parts per billion. Oxygen fugacity is fixed by $a(H_2S) = a(SO_4)^{2-}$ compatible with the common occurrence of gold in sulfide–sulfate assemblages. Thermodynamic data as for Figure 13.

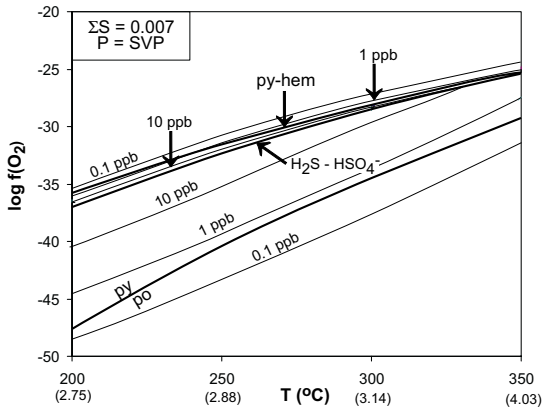

FIG. 15. Gold solubility as the AuHS° complex as a function of oxygen fugacity and temperature. Also shown are boundaries for selected iron sulfide and iron oxide minerals and the sulfate–sulfide boundary (heavy lines). The pH is given in parentheses below each temperature and reflects the decrease in pH accompanying conductive cooling of the PACMANUS vent fluid. The total reduced sulfur and pressure are the same as in Figure 13, as are the thermodynamic data.

rich mineral assemblages. In Zn-rich assemblages, grains of native gold occur predominantly as inclusions in tennantite that occupies an intermediate paragenetic position between early-formed chalcopyrite and later cavity-filling sphalerite. Gold in Cu-rich assemblages is present as micrometric grains included in massive chalcopyrite. This gold is primary, and is not the result of seafloor oxidation, as has been reported from the TAG (Hannington *et al.* 1988) and Logatchev (Murphy & Meyer 1998) hydrothermal fields.

The neutral AuHS° complex is considered the most important carrier of gold in the PACMANUS hydrothermal system. Such transport as a sulfide complex, rather than a chloride complex, is consistent with the high activity of sulfur indicated by the mineral assemblages associated with the gold mineralization, the coexisting iron-poor sphalerite and the Ag-poor nature of gold grains. Because the AuHS° complex is more stable than the $AuCl_2^-$ complex under all the conditions considered here, gold is precipitated from the sulfide complex in both Cu- and Zn-rich assemblages. Therefore, there is no need to rely on a low-temperature $Au(HS)_2^-$ complex and a high-temperature $AuCl_2^-$ complex for the respective Zn-rich and Cu-rich assemblages, as was proposed by Huston & Large (1989) for ancient massive sulfide deposits. Indeed, for the conditions considered here, Au(OH)° and not $AuCl_2^-$ is the most stable complex at temperatures greater than 325°C. This situation at Manus is probably common in all hydrothermal systems where fluids have a low pH, such as at Lau Basin (Fouquet *et al.* 1993) and Suiyo Seamount (Ishibashi *et al.* 1994). Precipitation of gold from such a hydrothermal fluid is mainly accomplished by a decrease in $a(H_2S)$ that may occur by mixing with seawater but, in shallow seafloor hydrothermal systems, may also result from loss of H_2S to a gas phase during boiling.

ACKNOWLEDGEMENTS

We are grateful to Anthony E. Williams-Jones for suggestions that improved an earlier version of this manuscript. Referees Ian R. Jonasson and J. Bruce Gemmell are thanked for their constructive comments and suggestions, which led to further improvements in the manuscript. The suggestions and careful editing of Robert F. Martin are gratefully acknowledged. This work was funded by a Natural Sciences and Engineering Research Council grant to SDS and by Ontario Graduate Student Scholarships to RM.

REFERENCES

ANDERSON, G.M. & CRERAR, D.A. (1993): *Thermodynamics in Geochemistry: the Equilibrium Model.* Oxford University Press, Oxford, U.K.

AUZENDE, J.-M., URABE, T. & SHIPBOARD SCIENTIFIC PARTY (1996a): Submersible observation of tectonic, magmatic and hydrothermal activity in the Manus Basin (Papua New Guinea). *Western Pacific Geophys. Meet.* (*Brisbane*), W115 (abstr.).

_____, _____ & _____ (1996b): Cruise explores hydrothermal vents of the Manus Basin. *Eos, Am. Geophys. Union Trans.* **77**, 244.

BARTON, P.B., JR. & TOULMIN, P., III (1964): The electrum-tarnish method for the determination of the fugacity of sulfur in laboratory sulfide systems. *Geochim. Cosmochim. Acta* **28**, 619-640.

_____ & _____ (1966): Phase relations involving sphalerite in the Fe–Zn–S system. *Econ. Geol.* **61**, 815-849.

BENES, V., SCOTT, S.D. & BINNS, R.A. (1994): Tectonics of rift propagation into a continental margin: western Woodlark Basin, Papua New Guinea. *J. Geophys. Res.* **99**, 4439-4455.

BENNING, L.G. & SEWARD, T.M. (1996): Hydrosulphide complexing of Au(I) in hydrothermal solutions from 150 to 400°C and 500 to 1500 bars. *Geochim. Cosmochim. Acta* **60**, 1849-1871.

BINNS, R.A. (1994): Submarine deposits of base and precious metals in Papua New Guinea. *In* Proc. PNG Geology, Exploration and Mining Conference. The Australasian Institute of Mining and Metallurgy, Melbourne, Australia (71-83).

_____ & SCOTT, S.D. (1993): Actively forming polymetallic sulfide deposits associated with felsic volcanic rocks in the eastern Manus back-arc basin, Papua New Guinea. *Econ. Geol.* **88**, 2226-2236.

_____, _____ & GEMMELL, J.B. (1997): Modern analogue of a mineral field: sea-floor hydrothermal activity hosted by felsic volcanic rocks in eastern Manus Basin, Papua New Guinea. *SEG Neves Corvo Field Conf.* (*Lisbon*), 33 (abstr.).

_____ & WHELLER, G.E. (1991): Report on the PACLARK-V/PACMANUS-I cruise, RV Franklin, Woodlark and Manus Basins, Papua New Guinea. *CSIRO Division of Exploration Geoscience, Restricted Rep.* **263R**.

BOTH, R., CROOK, K., TAYLOR, B., BROGAN, S., CHAPPELL, B., FRANKEL, E., LUI, L., SINTON, J. & TIFFIN, D. (1986): Hydrothermal chimneys and associated fauna in the Manus back-arc basin, Papua New Guinea. *Eos, Am. Geophys. Union, Trans.* **67**, 489-491 (abstr.).

COLE, D.R. & DRUMMOND, S.E. (1986): The effect of transport and boiling on Ag/Au ratios in hydrothermal solutions: a preliminary assessment and implications for the formation of epithermal precious metal ore deposits. *J. Geochem. Expl.* **25**, 45-80.

COOK, N.L. & CHRYSSOULIS, S.L. (1990): Concentrations of "invisible gold" in the common sulfides. *Can. Mineral.* **28**, 1-16.

CRAIG, H., CRAIG, V.K. & KIM, K.R. (1987b): PAPATUA Expedition 1: Hydrothermal vent surveys in back-arc basins: the Lau, N. Fiji, Woodlark, and Manus basins and Havre Trough. *Eos, Am. Geophys. Union, Trans.* **68**, 100 (abstr.).

_____, HORIBE, Y., FARLEY, K.A., WELHAN, J.A., KIM, K.R. & HEY, R.N. (1987a): Hydrothermal vents in the Mariana Trough: results of the first Alvin dives. *Eos, Am. Geophys. Union, Trans.* **68**, 1531 (abstr.).

_____ & POREDA, R. (1987): Studies of methane and helium in hydrothermal vent plumes, spreading axis basalts, and volcanic island lavas and gases in South West Pacific marginal basins. *Scripps Institute of Oceanography Ref.* **87-14**.

FOUQUET, Y., WAFIK, A., CAMBON, P., MEVEL, C., MEYER, G. & GENTE, P. (1993): Tectonic setting and mineralogical and geochemical zonation in the Snake Pit sulfide deposit (Mid-Atlantic Ridge at 23°N). *Econ. Geol.* **88**, 2018-2036.

GAMMONS, C.H. & WILLIAMS-JONES, A.E. (1995): The solubility of Au–Ag alloy + AgCl in HCl/NaCl solutions at 300°C: new data on the stability of gold(I) chloride complexes in hydrothermal fluids. *Geochim. Cosmochim. Acta* **59**, 3453-3468.

_____ & _____ (1997): Chemical mobility of gold in the porphyry-epithermal environment. *Econ. Geol.* **92**, 45-59.

_____, _____ & YU, Y. (1994): New data on the stability of gold(I) chloride complexes at 300°C. *Mineral. Mag.* **58A**, 309-310.

GAMO, T., OKAMURA, K., CHARLOU, J.L., URABE, T., AUZENDE, J.M., ISHIBASHI, J., SHITASHIMA, K., CHIBA, H. & SHIPBOARD SCIENTIFIC PARTY (1997): Acidic and sulfate-rich hydrothermal fluids from the Manus Back-arc basin, Papua New Guinea. *Geology* **25**, 139-142.

_____, SAKAI, H., ISHIBASHI, J., NAKAYAMA, E., ISSHIKI, K., MATSUURA, H., SHITATSHIMA, K., TAKEUCHI, K. & OHTA, S. (1993): Hydrothermal plumes in the eastern Manus Basin, Bismark Sea: CH_4, Mn, Al, and pH anomalies. *Deep Sea Res.* **40**, 2335-2349.

GENA, K, MIZUTA, T, ISHIYAMA, D., MATSUBAYA, O. & URABE, T. (1998): Mobility of major, minor and trace elements in basaltic andesite from a high sulfidation type of advanced argillic alteration in Desmos Caldera, Manus Basin, Papua New Guinea. *Geol. Soc. Am., Program Abstr.* **30**, A-127.

HANNINGTON, M.D., HERZIG, P.M., SCOTT, S.D., THOMPSON, G. & RONA, P.A. (1991): Comparative mineralogy and geochemistry of gold-bearing sulfide deposits on the mid-ocean ridges. *Marine Geol.* **101**, 217-248.

_____, _____ & STOFFERS, P. (1999): Submarine epithermal deposits: modern examples from Iceland, New Zealand, and Papua New Guinea. *Geol. Soc. Am., Program Abstr.* **31**, A-93.

_____, PETER, J.M. & SCOTT, S.D. (1986), Gold in sea-floor polymetallic sulfide deposits. *Econ. Geol.* **81**, 1867-1883.

_____ & SCOTT, S.D. (1988): Mineralogy and geochemistry of a hydrothermal silica – sulfide – sulfate spire in the caldera of Axial Seamount, Juan de Fuca Ridge. *Can. Mineral.* **26**, 603-625.

_____ & _____ (1989a) Gold mineralization in volcanogenic massive sulfides: implications of data from active hydrothermal vents on the modern sea floor. *Econ. Geol., Monogr.* **6**, 491-507.

_____ & _____ (1989b) Sulfidation equilibria as guides to gold mineralization in volcanogenic massive sulfides: evidence from sulfide mineralogy and the composition of sphalerite. *Econ. Geol.* **84**, 1978-1995.

_____, THOMPSON, G., RONA, P.A. & SCOTT, S.D. (1988): Gold and native copper in supergene sulphides from the Mid-Atlantic Ridge. *Nature* **333**, 64-66.

_____, TIVEY, M.K., LAROCQUE, A.C.L., PETERSON, S. & RONA, P.A. (1995): The occurrence of gold in sulfide deposits of the TAG hydrothermal field, Mid-Atlantic Ridge. *Can. Mineral.* **33**, 1285-1310.

HAYASHI, K.I. & OHMOTO, H. (1991): Solubility of gold in NaCl- and H_2S-bearing solutions at 250-350°C. *Geochim. Cosmochim. Acta* **55**, 2111-2126.

HELGESON, H.C. (1969): Thermodynamics of hydrothermal systems at elevated temperatures and pressures. *Am. J. Sci.* **267**, 729-804.

HERZIG, P.M., HANNINGTON, M.D., FOUQUET, Y., VON STACKELBERG, U. & PETERSON, S. (1993): Gold-rich polymetallic sulfides from the Lau backarc and implications for the geochemistry of gold in sea-floor systems of the southwest Pacific. *Econ. Geol.* **88**, 2182-2209.

HUSTON, D.L., BOTTRILL, R.S., CREELMAN, R.A., ZAW, K., RAMSDEN, T.R., RAND, S.W., GEMMELL, J.B., JABLONSKI, W., SIE, S.H. & LARGE, R.R. (1992): Geologic and geochemical controls on the mineralogy and grain size of gold-bearing phases, eastern Australian volcanic-hosted massive sulfide deposits. *Econ. Geol.* **87**, 542-563.

_____ & LARGE, R.R. (1989): A chemical model for the concentration of gold in volcanogenic massive sulfide deposits. *Ore Geol. Rev.* **4**, 171-200.

HUTCHINSON, R.W. (1990): Precious metals in massive base metal sulfide deposits. *Geol. Rundsch.* **79**, 241-263.

IIZASA, K., FISKE, R.S., ISHIZUKA, O., YUASA, M., HASHIMOTO, J., ISHIBASHI, J., NAKA, J., HORII, Y., FUJIWARA, Y., IMAI, A. & KOYAMA, S. (1999): A Kuroko-type polymetallic sulfide deposit in a submarine silicic caldera. *Science*, **283**, 975-977.

ISHIBASHI, J.I., TSUNOGAI, U., WAKITA, H., WATANABE, K., KAJIMURA, T., SHIBATA, A., FUJIWARA, Y. & HASHIMOTO, J. (1994): Chemical composition of hydrothermal fluids from the Suiyo and the Mokuyo Seamounts, Izu–Bonin Arc. *JAMSTEC J. Deep Sea Res.* **10**, 89-97 (in Japanese, with Engl. abstr.).

_____ & URABE, T. (1995): Hydrothermal activity related to arc–backarc magmatism in the western Pacific. *In* Backarc Basins: Tectonics and Magmatism (B. Taylor, ed.). Plenum Press, New York, N,Y. (451-495).

JOHNSON, J.W., OELKERS, E.H. & HELGESON, H.C. (1992): SUPCRT92: a software package for calculating the standard molal thermodynamic properties of minerals, gases, aqueous species, and reactions from 1 to 5000 bar and 0°C to 1000°C. *Computers Geosci.* **18**, 899-947.

KHARAKA, Y.K., GUNTER, W.D., AGGARWALL, P.K., PERKINS, E.H. & DEBRAAL, J.D. (1988): Solmineq.88: a computer program code for geochemical modeling of water–rock interactions. *U.S. Geol. Surv., Water Investigations Rep.* **88-4227**.

LARGE, R.R. (1990): The gold-rich massive sulphide deposits of Tasmania. *Geol. Rundsch.* **79**, 265-278.

LEISTEL, J.M., MARCOUX, E., DESCHAMPS, Y. & JOUBERT, M. (1998): Antithetic behaviour of gold in the volcanogenic massive sulphide deposits of the Iberian Pyrite Belt. *Mineral. Deposita* **33**, 82-97.

MARTINEZ, F. & TAYLOR, B. (1996) Backarc spreading, rifting, and microplate rotation, between transform faults in the Manus Basin. *Mar. Geophys. Res.* **18**, 203-224.

MOSS, R. & SCOTT, S.D. (1996): Silver in sulfide chimneys and mounds from 13°N and 21°N, East Pacific Rise. *Can. Mineral.* **34**, 697-716.

MURPHY, P.J. & MEYER, G. (1998): A gold–copper association in ultramafic-hosted hydrothermal sulfides from the Mid-Atlantic Ridge. *Econ. Geol.* **93**, 1076-1083.

SAKAI, H. (1991): Expedition East Manus Basin hydrothermal field, Hakuro–Maru Cruise KH90–3, Leg 2. A brief summary report for SOPAC: South Pacific Applied Geoscience Commision. *SOPAC Cruise Rep.* **138**.

SCOTT, S.D. & BARNES, H.L. (1971): Sphalerite geothermometry and geobarometry. *Econ. Geol.* **66**, 653-669.

_____ & BINNS, R. (1995): Hydrothermal processes and contrasting styles of mineralization in the western Woodlark and eastern Manus basins of the western Pacific. *In* Hydrothermal Vents and Processes (L.M. Parson, C.L. Walker & D.R. Dixon, eds.). *Geol. Soc., Spec. Publ.* **87**, 191-205.

SEWARD, T.M. (1991): The hydrothermal geochemistry of gold. *In* Gold Metallogeny and Exploration (R.P. Foster, ed.). Blackie and Sons, Glasgow, U.K. (37-62).

_____ & BARNES, H.L. (1997): Metal transport by hydrothermal fluids. *In* Geochemistry of Hydrothermal Ore Deposits (H.L. Barnes, ed.; third edition). John Wiley & Sons Inc., New York, N.Y. (435-486).

SILLITOE, R.H. (1989): Gold deposits in western Pacific island arcs: the magmatic connection. *Econ. Geol., Monogr.* **6**, 274-291.

SULEIMENOV, O.M. & SEWARD, T.M. (1997): A spectrophotometric study of hydrogen sulphide ionisation in aqueous solutions to 350°C. *Geochim. Cosmochim. Acta* **61**, 5187-5198.

SVERJENSKY, D.A., SHOCK, E.L. & HELGESON, H.C. (1997): Prediction of the thermodynamic properties of aqueous metal complexes to 1000°C and 5 kb. *Geochim. Cosmochim. Acta* **61**, 1359-1412.

TUFAR, W. (1990): Modern hydrothermal activity, formation of complex massive sulfide deposits and associated vent communities in the Manus back-arc basin (Bismarck Sea, Papua New Guinea). *Österreich. Geol. Gesellsch. Mitt.* **82**, 183-210.

WATANABE, K. & KAJIMURA, T. (1994): The hydrothermal mineralization at Suiyo Seamount in the Izu–Ogasawara arc. *J. Res. Geol.* **44**, 133-140 (in Japanese, with Engl. abstr.).

ZAW, K. & LARGE, R.R. (1996): Petrology and geochemistry of sphalerite from the Cambrian VHMS deposits in the Rosebery–Hercules district, Western Tasmania: implications for gold mineralization and Devonian metamorphic-metasomatic processes. *Mineral. Petrol.* **57**, 97-118.

ZOTOV, A.V., BARANOVA, N.N., DAR'YINA, T.G. & BANNYKH, L.M. (1991): The solubility of gold in aqueous chloride fluids at 350–500°C and 500–1500 atm: thermodynamic parameters of $AuCl_2$-(sol) up to 750°C and 5000 atm. *Geochem. Int.* **28**(2), 63-71.

_____, _____, _____, _____ & KOLOTOV, V.P. (1985): The stability of $AuOH^{\circ}_{sol}$ in water at 350–500°C and 500–1500 atm. *Geochem. Int.* **22**(5), 156-161.

Received November 4, 2000, revised manuscript accepted July 8, 2001.